Published in final edited form as:

Cell Rep. 2022 April 26; 39(4): 110745. doi:10.1016/j.celrep.2022.110745.

Critical contribution of 3′ non-seed base pairing to the *in vivo* function of the evolutionarily conserved *let-7a* microRNA

Ye Duan[1], **Isana Veksler-Lublinsky**[2], **Victor Ambros**[1,3,*]

[1]Program in Molecular Medicine, University of Massachusetts Chan Medical School, Worcester, MA 01605, USA

[2]Department of Software and Information Systems Engineering, Ben-Gurion University of the Negev, Beer-Sheva 8410501, Israel

[3]Lead contact

SUMMARY

Base pairing of the seed region (g2–g8) is essential for microRNA targeting; however, the *in vivo* function of the 3′ non-seed region (g9–g22) is less well understood. Here, we report a systematic investigation of the *in vivo* roles of 3′ non-seed nucleotides in microRNA *let-7a*, whose entire g9–g22 region is conserved among bilaterians. We find that the 3′ non-seed sequence functionally distinguishes *let-7a* from its family paralogs. The complete pairing of g11–g16 is essential for *let-7a* to fully repress multiple key targets, including evolutionarily conserved *lin-41*, *daf-12*, and *hbl-1*. Nucleotides at g17–g22 are less critical but may compensate for mismatches in the g11–g16 region. Interestingly, a certain minimal complementarity to *let-7a* 3′ non-seed sequence can be required even for sites with perfect seed pairing. These results provide evidence that the specific configurations of both seed and 3′ non-seed base pairing can critically influence microRNA-mediated gene regulation *in vivo*.

Graphical Abstract

*Correspondence: victor.ambros@umassmed.edu.

AUTHOR CONTRIBUTIONS

Conceptualization, Y.D., I.V.-L., and V.A.; methodology, Y.D., I.V.-L., and V.A.; formal analysis, Y.D., I.V.-L., and V.A.; investigation, Y.D. and I.V.-L.; resources, I.V.-L. and V.A.; data curation, Y.D.; writing – original draft, Y.D.; writing – review & editing, Y.D., I.V.-L., and V.A.; supervision, V.A.; project administration, V.A.; funding acquisition, V.A.

SUPPLEMENTAL INFORMATION

Supplemental information can be found online at https://doi.org/10.1016/j.celrep.2022.110745.

DECLARATION OF INTERESTS

The authors declare no competing interests.

INCLUSION AND DIVERSITY

One or more of the authors of this paper self-identifies as an underrepresented ethnic minority in science. The author list of this paper includes contributors from the location where the research was conducted who participated in the data collection, design, analysis, and/or interpretation of the work.

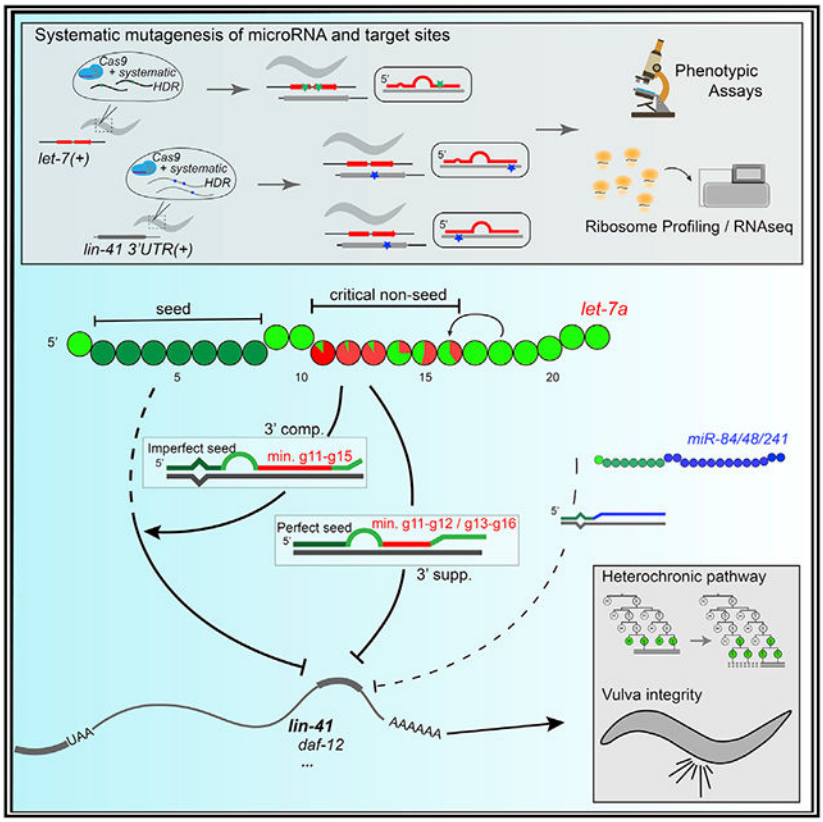

In brief

Duan et al. find that microRNA-target pairing at g11–g16 is critical for the function of evolutionarily conserved microRNA *let-7a*; 3′ pairing is required for both perfect and imperfect seed in regulating multiple targets. These findings provide evidence that base pairing of specific microRNA non-seed nucleotides can critically contribute to target regulation.

INTRODUCTION

MicroRNAs (miRNAs) are short non-coding RNAs found in all metazoans (Friedman et al., 2009; Lee et al., 1993; Nelson and Ambros, 2021). miRNAs are transcribed from specific genomic loci and processed into precursor miRNA (pre-miRNA) consisting of the miRNA and the passenger strand in a hairpin structure (Bartel, 2018). The pre-miRNA is further processed, and the mature miRNA binds Argonaute proteins (AGO) to form the miRNA-induced silencing complex (miRISC) and base pairs with complementary sites in the 3′ untranslated region (UTR) of target RNAs. miRISC binding leads to the repression of target gene expression through translational inhibition and/or target mRNA destabilization (Bartel, 2018). miRNAs are critical for the regulation of diverse physiological processes across species (Ambros, 2004; Bartel, 2018). miRNAs regulate an estimated 60% of human genes, and the dysfunction of miRNAs is implicated in multiple diseases (Friedman et al., 2009; Paul et al., 2018).

The miRNA seed corresponds to the 6–7 contiguous nucleotides beginning at the second nucleotide (g2) from the 5′ end. Structural and biochemical studies indicate that the miRNA seed sequence is critical for target recognition and determines miRNA targeting efficacy and specificity (Salomon et al., 2015; Schirle et al., 2014). Complementarity to the miRNA seed characterizes evolutionarily conserved miRNA target sites, and genetically disrupting seed complementarity results in target de-repression (Lai, 2002; Lewis et al., 2005; Lim et al., 2005).

Organisms commonly contain multiple genes encoding miRNAs with identical seed sequences, which are grouped into seed families. miRNAs with identical seeds can in principle recognize shared targets and function additively (Abbott et al., 2005; Alvarez-Saavedra and Horvitz, 2010; Brenner et al., 2012), while miRNAs with identical seed but divergent 3′ non-seed nucleotides (g9-g22) can select distinct target sites, driven by 3′ non-seed complementarity (Broughton et al., 2016; Wahlquist et al., 2014).

let-7 (lethal-7) family miRNAs are distributed widely across animal genomes, consistent with the origin of *let-7* in a bilaterian ancestor (Hertel et al., 2012; Wolter et al., 2017). The evolutionarily conserved developmental expression of *let-7 family* miRNAs, and the results from genetic analyses of *let-7 family* mutants, suggest the conservation of *let-7a family* functionality (Roush and Slack, 2008; Tennessen and Thummel, 2008). In nematodes, *let-7 family* miRNAs act in the heterochronic pathway to promote developmental cell fate transitions (Abbott et al., 2005; Reinhart et al., 2000). Similarly, *let-7 family* miRNAs control cellular transitions from pluripotency to differentiation in mammals and the timing of adult fates during metamorphosis in insects (Balzeau et al., 2017; Lee et al., 2016; Sokol et al., 2008).

Almost all bilaterian genomes encode at least one *let-7 family* isoform (*let-7a*), in which all nucleotides in the 3′ non-seed region are highly conserved (Figure S1A) (Hertel et al., 2012; Pasquinelli et al., 2003), suggesting that nucleotides g9-g22 of *let-7a* engage in critical interactions, which evolutionarily constrained the sequence. Indeed, data from genome-scale analyses of *in vivo* miRNA-target interactions support widespread miRNA 3′ non-seed pairing (Grosswendt et al., 2014; Helwak et al., 2013). Pairing to the 3′ non-seed region, especially g13-g16, is thought to enhance target repression in certain contexts (Brennecke et al., 2005; Grimson et al., 2007), and structural and biochemical studies of human AGO2 miRISC confirm that g13-g16 can form an A-form helix with the target to increase miRISC-target affinity and specificity (Sheu-Gruttadauria et al., 2019; Xiao and MacRae, 2020). Some miRNA target sites have imperfect seed complementarity accompanied by compensatory 3′ non-seed pairing, including *Caenorhabditis elegans lin-41*, for which 3′ non-seed pairing confers specificity for regulation by *let-7a* as opposed to other *let-7* family miRNAs (Chi et al., 2012; Doench and Sharp, 2004; Grimson et al., 2007; Vella et al., 2004). However, the relative contributions of specific 3′ non-seed nucleotides to the *in vivo* function of miRNAs remain unclear.

Here, we report a systematic investigation of how the 3′ non-seed nucleotides contribute to the *in vivo* function of *let-7a*. We used CRISPR-Cas9 genome editing of *C. elegans* to introduce defined mutations into *let-7a* or its conserved targets. Our results indicate that base

pairing of g11–g16 to targets is essential for *let-7a in vivo* function and that g17–g22 pairing is less critical than g11–g16 pairing but can partially compensate for mismatches in g11–g16. We confirm that the 3′ non-seed sequence of *let-7a* confers target specificity relative to its family paralogs. Furthermore, we show that *lin-41*, as well as heterochronic genes *daf-12* and *hbl-1*, are *let-7a* targets for which 3′ non-seed pairing is required. Interestingly, we find that the 3′ non-seed pairing to *let-7a* is functionally required in certain cases of perfect seed pairing, including the natural *daf-12* 3′ UTR and the reconfigured endogenous *lin-41* 3′ UTR, suggesting that the g11–g16 nucleotides of *let-7a* engage in essential interactions that, in parallel with seed pairing, critically influence miRISC activity.

RESULTS

The 3′ non-seed sequence is essential for the *in vivo* functional specificity of *let-7a* compared to family paralogs

The phylogenetic distribution of *let-7 family* miRNA genes among genomes with miRbase 22.1 annotations includes the vast majority of bilaterians (Figures 1A and S1B) (Kozomara et al., 2019). A total of 91.5% (n = 117) of bilaterian species have at least one *let-7 family* isoform with no more than 3 nucleotide differences from *hsa-let-7a* (Figure S1C). Alignment of the isoforms closest to *let-7a* from each of the 117 bilaterian species indicates that the g9–g22 nucleotides exhibit conservation ranging from 86% to 99%; 75.2% of these species contain a *let-7* family miRNA completely identical to *let-7a* (Figures 1B and S1F). This degree of conservation is not observed for other conserved miRNAs (Figures S1D-S1H). The deep conservation of *let-7a* suggests that *let-7a* is associated with essential functions that depend on the identity of the 3′ non-seed nucleotides.

To test whether *let-7a* 3′ non-seed nucleotides are critical for *in vivo* function, we used CRISPR-Cas9 to mutate the *let-7a* locus in *C. elegans* by swapping the *let-7a* sequence with that of its closest paralog *miR-84* (Figures 2A and S1A). The temporal expression profile of *miR-84* miRNA in *let-7(ma341)* is consistent with expression from the endogenous *mir-84* locus (starting in the larvalL2 stage) combined with expression from the edited *let-7* locus (peaking in the L4 stage) (Figures 2B and 2C). Meanwhile in the *mir-84(n4037, null)* background, *miR-84* expression from the *let-7(ma341)* locus exhibits a temporal profile like that of normal *let-7a* (Figures 2D-2E), suggesting that *miR-84* miRNA is expressed from the endogenous *let-7* locus.

In wild-type (WT) larvae, seam cells (hypodermal stem cells) undergo asymmetric divisions at each larval stage: one daughter cell differentiates to Hyp7 cells (hypodermis), while the other remains a stem cell (Sulston et al., 1983). At the L4 molt, the seam cells exit the cell cycle, fuse, and produce an adult-specific cuticle structure, the lateral alae. *let-7(ma341)* animals exhibit heterochronic and vulva integrity defects like *let-7 loss-of-function (lf)*, including an extra round of seam cell division after the L4 molt, incomplete adult lateral alae (Figures 2F and 2G; Table S1), reduced expression of the adult-specific hypodermal reporter COL-19::GFP (Figures 2H and 2I), and adult lethality caused by bursting at the vulva (Figures 2J-2L). These phenotypes are consistent with the *let-7a lf* phenotypes observed in the *null (ma393)* and seed (*n2853*) mutants, indicating that the *in vivo* function of *let-7a* cannot be substituted by its closest paralog *miR-84*, even when *miR-84* is expressed in a

developmental profile essentially identical to *let-7a* (Liu et al., 1995; Nelson and Ambros, 2019; Reinhart et al., 2000). Since *let-7a* and *miR-84* share the same seed sequence, these findings indicate that the 3′ non-seed sequence is a critical determinant of the *in vivo* function and specificity of *let-7a*.

Nucleotides 11–16 are each functionally essential for *let-7a in vivo*

To characterize how each 3′ non-seed nucleotide contributes to the *in vivo* function of *let-7a*, we performed a single-nucleotide mutational screen using the "jump-board" strategy (Duan et al., 2020a). For each g9–g22 nucleotide, we mutated both the miRNA and passenger strands to preserve the pre-miRNA structure (Figures 3A and S2A). To confirm the expression of the mutant miRNAs, we performed small RNA sequencing of all of the mutants and found that the abundance of the mutated *let-7a* miRNA in all cases was greater than 50% of that of the native *let-7a* in WT (Figure 3B). Since *let-7* is recessive in *C. elegans* (indicating that the 2-fold reduction of *let-7a* dosage is not phenocritical), we reason that any phenotypes exhibited by these mutants can be attributed to the sequence of the miRNA, not reduced expression. Note that the strains with mutations at g11–g13 also contained a WT *let-7* allele on a genetic balancer *umnIs25(mnDp1);* hence, both WT and mutant *let-7a* were expressed.

Single-nucleotide mutations at g11, g12, or g13 resulted in severe vulva integrity defects, leading to lethality and dramatically reduced fecundity similar to *let-7(null)* (Figures 3C and 3D). Mutation of g11, g12, or g13 also caused defects in adult alae morphogenesis and COL-19::GFP expression, which are indicative of retarded heterochronic phenotypes (Figures 3C and S2B; Table S1). Single-nucleotide mutations at g14–g16 also resulted in distinct *let-7a lf* phenotypes, although they were milder than g11–g13 mutations (Figures 3C-3E). By contrast, single-nucleotide mutations at g9–g10 or g17–g22 did not cause visible phenotypes (Figures 3C-3F; Table S1). These results reveal g11–g16 to be a critical non-seed region of *let-7a*, with g11–g13 relatively more essential than g14–g16 (Figure 3I).

Nucleotides beyond g16 can compensate for mismatches in the critical non-seed region

Mutation of g18 to any of the other 3 nucleotides did not result in *let-7a lf* phenotypes, nor did simultaneous mutation within the g17–g22 region of 3 (g17–g19 or g20–g22) or 6 (g17–g22) consecutive nucleotides (Figure S2C). These results stand out in contrast to the deep conservation of the *let-7a* g17–g22 sequence (Figure 1B). We hypothesized that g17–g22 may contribute to target repression in cases in which mismatches occur within the g11–g16 region. To test this possibility, we generated a compound mutant *let-7(ma449ma435)* with both U16G and U18A mutations. We observed that *let-7(ma449ma435)* exhibited vulva bursting and retarded adult alae phenotypes (Figures 3E-3H, S2C, and S2D) that were significantly more penetrant than for each single mutant alone. We conclude that g18, and by implication other g17–g22 nucleotides, may contribute to interactions that involve mismatches in the g14–g16 subcritical region.

It is also possible that g17–g22 pairing could be critical for target repression associated with phenotypes that we have not measured. We accordingly assessed molecular phenotypes of *let-7(ma435)* by ribosome profiling and RNA sequencing (RNA-seq) (Figure S3; Table S2).

We found that the expression levels of multiple genes are significantly changed by the U18A mutation, including 3 putative *let-7a* targets with predicted pairing to g18, supporting the hypothesis that there are *in vivo* circumstances in which g17–g22 nucleotides are critical for proper target regulation.

De-repression of *lin-41* is a major contributor to *let-7a* critical non-seed mutant phenotypes

The evolutionarily conserved gene *lin-41/Trim71* is a direct target of *let-7a* across diverse phyla, and repression of *lin-41/Trim71* by *let-7a* is essential for normal development in invertebrates and vertebrates (Ecsedi and Grosshans, 2013; Worringer et al., 2014). In *C. elegans*, robust repression of *lin-41* by *let-7a* is critical for the L4-to-adult cell fate progression, and mutations disrupting the seed pairing between *let-7a* and its 2 complementary sites (LCSs) in the *lin-41* 3′ UTR result in the reiteration of L4 cell fates and severe vulva defects (Aeschimann et al., 2019). Notably, both *lin-41* LCSs have imperfect seed complementarity to *let-7a* with a GU pair and a target A-bulge, respectively, and both LCSs contain complementarity to *let-7a* g11-g19, suggesting that 3′ pairing is essential to compensate for weak seed pairing to *lin-41* mRNA (Figure 4A).

We sought to verify whether the *lf* phenotypes of *let-7a* critical non-seed mutants result from de-repression of *lin-41*. We used the *ma432*(U13A) mutant to represent the critical non-seed nucleotides due to its severe phenotypes and the relatively high conservation of g13. At the late L4 stage of WT, endogenously tagged GFP::LIN-41 is undetectable in hypodermal cells due to *let-7a* repression (Figure S4A) (Spike et al., 2014). In contrast, in *let-7(ma432,g13)*, we observed elevated peri-nuclear expression of GFP::LIN-41 in seam and Hyp7 cells, suggesting the de-repression of *lin-41* (Figure S4B). To confirm that the *lin-41* de-repression in *let-7(ma432,g13)* results specifically from the disruption of g13 pairing, we restored the native pairing configurations between *let-7(ma432,g13)* and *lin-41* by introducing compensatory mutations at both LCSs in *lin-41* 3′ UTR (*ma480,t13*) (Figure 4A). GFP::LIN-41 expression was not detectably elevated in *lin-41(ma480,t13);let-7(ma432,g13)*, indicating that restoring g13:t13 pairing restored *lin-41* repression (Figure S4C). Using qRT-PCR and ribosome profiling, we confirmed that the levels of *lin-41* mRNA abundance and translation were elevated in *let-7(ma432,g13)* compared to the WT, and restored to normal levels in *lin-41(ma480,t13);let-7(ma432,g13)* (Figure S4E and S6A). In *lin-41(ma480,t13);let-7(ma432,g13)* animals, the *let-7(lf)* phenotypes caused by the *ma432* mutation were substantially rescued, based on the reduced lethality, increased number of progeny, and normal adult alae (Figures 4B-4F; Table S1). The rescue of *let-7(ma432,g13)* phenotypes by restoring non-seed pairing indicates that de-repression of *lin-41* is the major contributor to the *lf* phenotypes of *let-7a* critical non-seed mutants.

In parallel, we found that when present with WT *let-7a, lin-41(ma480,t13)* exhibited an elevated peri-nuclear expression of GFP::LIN-41, suggesting that disrupting the critical non-seed pairing by mutations in the target also causes *lin-41* de-repression (Figure S4D). As expected, we also observed vulva integrity defects and retarded heterochronic phenotypes in *lin-41(ma480)* (Figures 4E and 4F; Table S1), supporting the conclusion that 3′ non-seed

pairing between *let-7a* and *lin-41* is essential for the developmental down-regulation of *lin-41*.

Disruption of *let-7a* 3′ non-seed pairing results in de-repression of additional targets, including *daf-12* and *hbl-1*

Although *lin-41(ma480,t13);let-7(ma432,g13)* showed reduced *lf* phenotypes compared to *let-7(ma432,g13)*, the double mutant exhibits residual defects in vulva morphogenesis and egg-laying capacity (Figures 4D-4F) and reduced COL-19::GFP expression in Hyp7 cells of adults at 25°C, indicating residual retarded heterochronic phenotypes (Figure 4G). These residual phenotypes suggest that although *lin-41(ma480,t13);let-7(ma432,g13)* restores *lin-41* repression, the *let-7(ma432)* mutation may cause de-repression of additional targets that require critical non-seed pairing, referred to here as "3′ targets" (Figure 4H). Consistent with the reasoning that the phenotypes of *let-7(ma432,g13)* result from the combined overexpression of *lin-41* and other 3′ targets, the *lin-41(ma480,t13)* single mutant, in which *lin-41* is the only *let-7a* 3′ target expected to be overexpressed, exhibits weaker phenotypes than *let-7(ma432,g13)* (Figure 4F; Table S1).

To identify *let-7a* 3′ targets in addition to *lin-41*, we screened for genes that are de-repressed by the *let-7a* critical non-seed mutation using ribosomal profiling (Ribo-seq), which assesses gene expression on the translational level (Ingolia, 2016). We compared Ribo-seq profiles between WT and *lin-41(ma480,t13);let-7(ma432,g13)*, in which *lin-41* repression is restored, yet other *let-7a* 3′ targets are expected to be de-repressed. At the L4 stage, 351 genes were significantly overexpressed >1.5-fold in *lin-41(ma480,t13);let-7(ma432,g13)*. To apply a stringent test for which of these differentially expressed genes could be perturbed as a result of the *let-7a* mutation specifically versus genes whose observed perturbation could be caused by asynchrony in staging between samples, we applied a filter to remove genes that are known to be highly dynamic over the developmental interval encompassing our sample collections (Aeschimann et al., 2017) (STAR Methods). A total of 203 genes passed this filter and were therefore judged to be likely overexpressed due to the *let-7a* mutation specifically (Figure 5A; Table S3). The translational levels of *lin-41* and its direct downstream genes were not significantly changed compared to WT, indicating that the de-repressed genes in *lin-41(ma480,t13);let-7(ma432,g13)* are independent of *lin-41* pathway (Figure S6A) (Aeschimann et al., 2019). To identify potential direct *let-7a* 3′ targets among the overexpressed genes, we used a computational approach to predict *let-7a* sites using seed pairing and g11–g16 pairing constraints (STAR Methods) (Veksler-Lublinsky et al., 2010). We identified 624 *C. elegans* genes whose 3′ UTRs contain *let-7a* 3′ sites, among which 8 genes are overexpressed in the g13 mutant, including the heterochronic genes *daf-12* and *hbl-1* (Figure 5A; Table S4).

The 3′ UTRs of *daf-12* and *hbl-1* contain multiple *let-7a* sites with complementarity to the critical non-seed region of *let-7a* (Figures S6B-S6D). We reasoned that the de-repression of *daf-12* and/or *hbl-1* could contribute to the residual heterochronic phenotypes of *lin-41(ma480,t13); let-7(ma432,g13)*. Therefore, we used RNAi to knock down *daf-12* or *hbl-1* during the larval development of *lin-41(ma480,t13);let-7(ma432,g13)* and assayed for suppression of the residual *lf* phenotypes. Knocking down either *daf-12* or *hbl-1* by RNAi

rescued the abnormal COL-19::GFP pattern in *lin-41(ma480,t13);let-7(ma432,g13)* (Figure 5B), suggesting that de-repression of *daf-12* and *hbl-1* contributes to the residual retarded phenotypes of *lin-41(ma480,t13);let-7(ma432,g13)*, and that the critical non-seed pairing of *let-7a* is required for the repression of not only *lin-41* but also additional targets, including *daf-12* and *hbl-1*, for the L4-to-adult transition.

Previous transgenic reporter analyses suggested that *daf-12* can be repressed by *let-7* family miRNAs during larval development (Grosshans et al., 2005; Hammell et al., 2009). To gather additional evidence in support of a role for *let-7a* in the downregulation of DAF-12, we quantified the level of expression of an endogenously tagged fluorescent reporter *daf-12(ma498,-mScarlet)* (Ilbay and Ambros, 2019) in the L3 and L4 stages, which span the interval when *let-7a* is dramatically upregulated. The data confirm that endogenous DAF-12::mSCARLET expression is significantly downregulated in seam cells between the L3 and L4 stages, consistent with the repression of *daf-12* by *let-7a* in the L4 (Figures 5D, 5F, 5G, S7B, and S7C).

To further test whether 3′ pairing to *let-7a* is required for the developmental downregulation of DAF-12, we used CRISPR-Cas9 editing to mutate the LCS sequences in the endogenous *daf-12(ma498,mScarlet)* 3′ UTR (Figure S7A) to disrupt *let-7a* g11-g13 complementarity. We found that compared to WT, the L4-specific reduction of DAF-12::mSCARLET in seam cells was abrogated in *daf-12(ma498ma568)* larvae (Figures 5E-5G). Thus, we conclude that 3′ non-seed pairing of *let-7a* contributes to the repression of *daf-12* at the L4 stage.

daf-12(ma498ma568) exhibits a retarded COL-19::GFP expression phenotype (Figure 5H), supporting the idea that de-repression of *daf-12* contributes to the residual phenotypes of *lin-41(ma480);let-7(ma432)*. Meanwhile, *daf-12(ma498ma568)* exhibits relatively less penetrated phenotypes (4.6%, Figure 5H) compared to *lin-41(ma480);let-7(ma432)* (76.6%; Figure 5B), suggesting that the L4-to-adult cell fate transition requires the downregulation of multiple 3′ targets in addition to *lin-41* and *daf-12*, such as *hbl-1* (Figure S7E).

Repression of *let-7a* 3′ targets can involve translational suppression and/or mRNA decay

miRNA-mediated gene regulation can occur via translational repression or mRNA destabilization, indicated by decreased translational efficiency (TE) or reduced mRNA abundance, respectively (Bazzini et al., 2012; Giraldez et al., 2006). *let-7a* appears to regulate *lin-41* through a combination of both modes (Bagga et al., 2005; Nottrott et al., 2006). To assess the repression mechanisms for 3′ targets other than *lin-41*, we performed Ribo-seq and RNA-seq analyses of *lin-41(m480,t13);let-7(ma432,g13)* at L4 larvae (Figures 5C and S6; Table S3). We found that the set of de-repressed *let-7a* 3′ targets in *lin-41(ma480,t13);let-7(ma432,g13)* included examples of increased mRNA abundance (e.g., *grd-10*) or increased TE (e.g., *hbl-1*), or a combination of both (e.g., *daf-12*) (Figure 5C). The verified *let-7a* targets *daf-12* and *hbl-1* were de-repressed in the same fashion as reported previously for seed mutants (Aeschimann et al., 2017) (Figure S5H). Thus, target recognition involving the *let-7a* 3′ non-seed region can elicit inhibition of TE or mRNA stability or both.

Continuous pairing at g11–g15 is required to compensate for the imperfect seed pairing between *let-7a* and *lin-41*

The involvement of 3′ pairing to compensate for imperfect seed pairing can be essential for *in vivo* targeting efficacy for certain miRNA-target interactions, but how the base pairing at different positions contributes to this compensatory effect remains unclear (Bartel, 2018). Moreover, detailed analyses of how 3′ pairing contributes to endogenous target repression in the context of perfect seed pairing are lacking. To investigate how 3′ pairing coordinates with seed pairing for endogenous target repression, we systematically introduced mutations designed to produce various configurations of seed and non-seed pairing between WT *let-7a* and the *lin-41* 3′ UTR (Figure 6). In each case, mutations were introduced into both *lin-41* LCSs and were tested in the WT *let-7a* background, so the observed phenotypes should reflect the de-repression of *lin-41* without confounding effects from other *let-7a* targets.

A previous study using mutant *lin-41* LCS constructs with *let-7a* 3′ complementarity restricted to g13–g16 found that g13–g16 pairing alone was insufficient to compensate for imperfect seed pairing (Brancati and Grosshans, 2018). Our finding that certain single mismatches at g13 can cause strong *lin-41 gain-of-function (gf)* phenotypes suggests that the extent of 3′ pairing is less important than the precise pattern of pairing (Figure 6E). Through further analysis of a series of single-nucleotide mutations in the *lin-41* 3′ LCSs (Figure 6G), we found that disrupting base pairing at any single position in the g11–g15 complementary region results in *lin-41 gf* phenotypes, indicating that continuous pairing from g11 to g15 is required to compensate for the imperfect seed pairing between *let-7a* and *lin-41* (Figure 6I).

To determine whether the requirement for g11–g15 pairing is to compensate for the imperfect seed match characteristic of the WT *lin-41:let-7a* interaction, we mutated both LCSs of the t11, t12, and t13 *lin-41* mutants to permit consecutive g2–g8 Watson-Crick pairing (PS) to *let-7a*, while maintaining the single 3′ mismatch in each case. We found that the resulting compound mutants *lin-41(ma501ma555,PS + t11), lin-41(ma501ma556,PS + t12)*, and *lin-41(ma501ma480,PS + t13)* exhibited substantial rescue of the *gf* phenotypes of *lin-41(ma555,t11), lin-41(ma556,t12)*, and *lin-41(ma480,t13)*, respectively (Figures 6B and 6H). This finding suggests that the requirement for pairing across g11–g15 in large part reflects compensation for imperfect seed pairing of *let-7a* to the *lin-41* WT LCSs.

Both seed and 3′ non-seed pairing of *let-7a* are required for full repression *lin-41*

The above results suggest that the requirements for 3′ pairing may be less stringent with a perfect seed pairing to *let-7a* compared to the imperfect seed. To test whether 3′ pairing in the g11-g13 region is fully dispensable in the context of perfect seed pairing, we combined *ma501* with a compound mutation *(ma545)* which simultaneously mismatches g11–g13 of *let-7a* (Figure 6C). Interestingly, *lin-41(ma501ma545,PS + t11–13)* exhibited strong vulva integrity defects and retarded COL-19::GFP expression, indicating that *lin-41* was de-repressed despite the perfect seed pairing to *let-7a* (Figure 6C). This indicates that even with perfect seed complementarity, pairing within g11–g13 still critically contributes to the functional targeting of *lin-41*. We also combined *ma501* with mismatch mutations at *t11–t12* and *t13–t16*. The resulting mutants *lin-41(ma501ma571,PS + t11–t12)* and *lin-41(ma501ma572,PS + t13–t16)* did not exhibit observable *lin-41 gf* phenotypes (Figure

6H). We suggest that in the context of perfect seed pairing, full *lin-41* repression by *let-7a* can occur provided that there is 3′ pairing at g11–g12 (*lin-41(ma501ma572)*) or g13–g16 *(lin-41(ma501ma571))* (Figure 6I).

These results suggest that *let-7a* family paralogs *miR-48, miR-84*, and *miR-241*, which differ from *let-7a* substantially in their 3′ sequences, should not fully repress *lin-41* even with engineered perfect seed pairing, even though their combined expression may exceed the level of *let-7a* at the L4 stage in *C. elegans* (Nelson and Ambros, 2021) (Figures 7A and 7C). Accordingly, *lin-41(ma501,PS);let-7a(ma393,null)* exhibited vulva integrity defects nearly as severe as *let-7a(ma393,null)*, indicating that *let-7a* family paralogs do not contribute substantially to *lin-41* repression, even with engineered perfect seed matches (Figure 7B).

The evident importance of 3′ pairing for *lin-41* repression by *let-7a* prompted us to test whether 3′ non-seed pairing could compensate for severely compromised seed pairing. We used a previously reported allele *lin-41(xe11)*, which creates 2 consecutive seed mismatches to *let-7a* in each LCS (Ecsedi et al., 2015). We confirmed that *lin-41(xe11)* animals exhibit strong vulva integrity defects and retarded heterochronic phenotypes (Figure 6F), indicating that extensive 3′ pairing does not render seed pairing dispensable.

DISCUSSION

A 6-nt critical non-seed pairing region of *let-7a*, involving g11–g16

Base paring of the 3′ non-seed region of miRNAs to targets has been implicated in compensating for weak seed pairing, for seed family isoform specificity, and target-dependent miRNA degradation (TDMD) (Bartel, 2018; Pawlica et al., 2020). However, there has been no systematic study of the contribution of individual 3′ non-seed nucleotides to the functional efficacy of miRNA-target interactions in intact animals. The functional contributions of individual 3′ nucleotides is particularly pertinent for miRNAs with evolutionarily conserved 3′ non-seed sequences (e.g., *let-7a*) and for their evolutionarily conserved targets (e.g., *lin-41*, in the cae of *let-7a*). Here, we used CRISPR-Cas9 genome editing for a systematic investigation of the *in vivo* function of individual 3′ non-seed nucleotides of *let-7a* in the regulation of *lin-41* and other targets in *C. elegans*.

A key finding from our studies is that each nucleotide at g11–g16 critically contributes to the *in vivo* function of *let-7a*. This is consistent with findings from human miRISC *in vitro* RNA bind-n-seq (RBNS) showing that pairing to g11–g16 of *let-7a* is particularly crucial for enhancing the affinity of miRISC for oligonucleotide targets (McGeary et al., 2022). We further found that within g11–g16, the g11–g13 subregion is particularly important to *let-7a in vivo* function. This finding also agrees with the RBNS results, which show that among 4-nt blocks of target complementarity scanned along the *let-7a* 3′ region, pairing at g11–g14 was the most potent contributor to enhanced target affinity (McGeary et al., 2022). Therefore, both our genetic analysis in *C. elegans* and the RBNS analysis of human AGO2 agree on a 6-nt critical 3′ pairing region (g11–g16) of *let-7a*, expanded by 2 nt compared to the g13–g16 region previously identified by biochemical analysis and the co-crystallized

structure of the miRISC-target complex (Grimson et al., 2007; Sheu-Gruttadauria et al., 2019).

Our results stand in contrast to a previous genetic study that indicated the functional insignificance of the 3′ non-seed region of *let-7a* in *C. elegans*, in which a compound mutation at g10, g12, and g13 of *let-7a* exhibited relatively mild developmental defects (Zhang et al., 2015). It is likely that since the results from Zhang et al. (2015) were obtained using exogeneous high-copy transgenes to express mutant *let-7a* miRNAs, the overexpression of the mutant miRNA compensated for its poor intrinsic efficacy. This highlights the importance of using genome engineering of endogenous miRNA loci so that repression efficacy can be assessed in the context of native gene dosage.

Structural analyses of human miRISC reveal that duplexing of a miRNA with perfect seed complementarity to target results in 3′ pairing at g13–g16, while g11 and g12 were structurally hindered from duplexing with the target (Sheu-Gruttadauria et al., 2019). Our results suggest that for certain target interactions, *let-7a*-miRISC may adopt a previously unanticipated conformation that enables g11–g16 pairing to target. For the evolutionarily conserved *let-7a* target *Trim71/lin-41*, LCS sequences conserve the combination of imperfect seed pairing accompanied by 3′ pairing involving g11 and g12. In some instances, even the specific configuration of seed mismatches is conserved (Nelson and Ambros, 2021)). We suggest that these mismatched seed configurations may promote an AGO conformation that favors the pairing of g11–g12, in addition to the previously identified g13–g16 pairing.

Although our results confirm that certain imperfect seed match configurations can be compensated for by extensive 3′ pairing, we also confirm that seed pairing is not dispensable, as *lin-41* LCSs with 2 nt seed mismatches displayed strong *lin-41 gf* phenotypes despite extensive 3′ pairing (Figure 6F). Similarly, disrupting either the seed or 3′ complementarity results in de-repression of *daf-12* in *C. elegans* (Figure S7D) (Aeschimann et al., 2017).

Contribution of the 3′ non-seed pairing to the target specificity of *let-7* family paralogs

Broughton et al. (2016) reported that the *C. elegans let-7a* family paralog *miR-48*, which does not regulate *lin-41* in WT, can substitute for *let-7a* in repressing *lin-41* if the *lin-41* LCSs were replaced by sites with perfect seed match plus 3′ pairing to *miR-48*. It was proposed that the weak seed pairing of *let-7a* to *lin-41* necessitates the 3′ pairing, which differs remarkably between *let-7a* and *miR-48*, and consequently determines the targeting specificity whereby *lin-41* is regulated by *let-7a*, not *miR-48* (Brancati and Grosshans, 2018). Thus, 3′ non-seed pairing combined with imperfect seed pairing is a powerful determinant of specificity for miRNAs of the same seed family. This model is supported by our finding that *miR-84*, the closest family paralog of *let-7a* in *C. elegans*, does not functionally substitute for the absence of *let-7a* (Figure 2). We suggest that our result provides a stringent test of the model, because in our experiments, *miR-84* was expressed at levels and with a temporal profile identical to WT *let-7a;* and unlike *miR-48* in the previous reports, which differs from *let-7a* at every non-seed position, *miR-84* has only 5 nt different from *let-7a* (Figure S1A). We also confirm that the *in vivo* functional distinction between

let-7a and *miR-84* primarily reflects the specificity of *let-7a* for targeting *lin-41*, as well as other targets that require 3′ non-seed pairing (Figure S5).

By mediating miRNA family targeting specificity, 3′ non-seed pairing may enable spatiotemporal specificity of target regulation. In *C. elegans, hbl-1* is repressed by *let-7a* paralogs at the L2-to-L3 transition, and by *let-7a* at the L4-to-adult transition (Abrahante et al., 2003; Ilbay and Ambros, 2019). The *hbl-1* 3′ UTR has sites with perfect seed match that can be recognized by any paralog in the *let-7 family* (perfect seed only), and hence may mediate the repression of *hbl-1* by *let-7 family* paralogs at earlier larval stages. Meanwhile, the *hbl-1* 3′ UTR also contains sites expected to be specifically recognized by *let-7a* (imperfect seed +3′ pairing), which enables the *let-7a*-specific repression of *hbl-1* in cells that express *let-7a* at late larval stages (Figure S6D).

The necessity of 3′ non-seed pairing for target repression in the context of perfect seed pairing

It has long been recognized that perfect seed complementarity can be sufficient, in certain contexts, for miRISC to bind and repress a target (Brennecke et al., 2005; Doench and Sharp, 2004; Wee et al., 2012), implying that 3′ pairing may be required only to compensate for weak seed pairing. However, there is also evidence that 3′ pairing can contribute critically to target regulation for instances of perfect seed matches. For example, evolutionarily conserved target sites with perfect seed plus 3′ pairing (3′ supplemental sites) are prevalent in metazoan clades and appear to be more frequent than the 3′ compensatory sites, which have imperfect seed pairing (Friedman et al., 2009). Also, competitive binding experiments reveal that 3′ pairing can enhance miRISC affinity to perfect seed sites and enable miRNA isoforms with identical seeds to compete for target recognition (Xiao and MacRae, 2020).

Broughton et al. (2016) reported findings indicating that in the context of perfect g2–g7 seed pairing, 3′ pairing is required for the specificity of *C. elegans let-7 family* isoforms in the developmental repression of *lin-41*. Brancati and Grosshans (2018) showed that for *lin-41* LCSs modified to contain a modified *miR-48* site from the *dot-1.1* gene with perfect g2–g8 *let-7a* seed pairing, *let-7a* was unable to fully rescue the *mir-48(null)* phenotypes. Our results reinforce those findings by showing that in the absence of *let-7a, the let-7 family* paralogs can only confer a limited degree of repression of *lin-41* via perfect seed pairing alone (Figure 7). Moreover, we investigated the minimal requirements for 3′ pairing for the full repression of *lin-41* containing LCSs with perfect g2–g8 seed pairing and confirmed that specific *let-7a* 3′ pairing is necessary to supplement perfect g2–g8 pairing, but the functional constraints on 3′ pairing are less stringent for the perfect seed pairing (Figure 6). Importantly, we show that the WT 3′ UTRs of additional *let-7a* targets, including the heterochronic gene *daf-12*, contain sites with perfect seed matches combined with extensive 3′ complementarity to *let-7a*, and the 3′ supplemental pairing is essential for the downregulation of DAF-12 at later developmental stages (Figure 5). These findings run counter to the assumption that perfect seed pairing should be sufficient for miRISC to confer repression and emphasize that in the native context of an intact developing animal,

the miRNA 3′ non-seed pairing can be critical for the efficacy of evolutionarily conserved miRNA-target interactions.

It is noteworthy that the LCSs with perfect seed plus 3′ complementarity to *let-7a* in the *daf-12* 3′ UTR should also allow binding of the *let-7* family paralogs by seed pairing. Indeed, it has been reported that *daf-12* is repressed by *let-7* family paralogs (*mir-48*, *mir-84*, *mir-241*) at the L2-to-L3 stage transition, and by *let-7a* at the L4 stage (Grosshans et al., 2005; Hammell et al., 2009) (Figures 5D-5F). Since 3′ pairing can render higher target binding affinity to the miRISC, we suggest that the involvement of 3′ non-seed pairing to *let-7a* may enable more efficacious repression of *daf-12* at the L4 stage than that at earlier stages (Figure 5G).

Currently, we can only speculate about the mechanistic basis for this requirement for 3′ pairing in the context of perfect seed match. Perhaps certain structural peculiarities of a 3′ UTR (e.g., *daf-12, lin-41*) may render *let-7a* "seed-only" pairing unfavorable compared to "seed plus 3′ supplemental" pairing, or even "imperfect seed plus 3′ compensatory" pairing. It is also possible that repression by *let-7a* requires the recruitment of cofactors that recognize miRISC conformational features induced by 3′ pairing.

The multiplicity of *C. elegans let-7a* targets with 3′ non-seed pairing

Previous reports showed that *lin-41* is the major *let-7a* target whose de-repression underlies the *lf* phenotypes of *let-7a* seed mutants (Ecsedi et al., 2015). In our study, we further confirmed that *lin-41* is the major *let-7a* 3′ target by showing the de-repression of LIN-41 by a g13 mutation *let-7(ma432)*, and the rescue of LIN-41 de-repression and the associated *lf* phenotypes by a compensatory mutation *lin-41(ma480)*. These results were assessed using 3 approaches: (1) an endogenously tagged fluorescent LIN-41 reporter for the visualization of cell-specific expression (Figures S4A-S4D); (2) qRT-PCR to measure the global level of *lin-41* transcript (Figure S4E); and (3) ribosome profiling to measure the global level of translation of *lin-41* mRNA (Figure S6A). Note that we were not able to analyze the *let-7(ma432)* single mutant because *let-7(ma432)* animals exhibit strong adult lethality, which precludes propagating them in numbers that are adequate for ribosome profiling. However, a previous report showed that the translational level of *lin-41* was upregulated approximately 8 times in the *let-7(n2853)* seed mutant (Aeschimann et al., 2017). Since *let-7(ma432)* exhibits stronger phenotypes than does *let-7(n2853)*, we anticipate that *lin-41* should be overexpressed to a greater degree in *let-7(ma432)* than in *let-7(n2853)*. Thus, the non-significant changes in ribosome-protected footprint for *lin-41* in *lin-41(ma480);let-7(ma432)* animals (Figure S6A) can be interpreted to indicate the restoration of normal *lin-41* repression.

Our computational analysis identified 624 genes in *C. elegans* that contain 3′ UTR sequences predicted to bind *let-7a* with 3′ non-seed pairing. This finding is consistent with previous high-throughput analyses of miRNA-target chimeric ligation products, which also identified multiple *let-7a* targets with 3′ non-seed complementarity (Broughton et al., 2016; Grosswendt et al., 2014). By ribosome profiling, we confirmed that 3′ non-seed pairing is critical for the *let-7a* repression of at least 8 genes and that the overexpression of *daf-12* and *hbl-1* contribute to the developmental phenotypes of the *let-7a* g13 mutant

(Figure 5). This finding indicates that in addition to *lin-41*, at least *daf-12* and *hbl-1* are also phenocritical *let-7a* targets in *C. elegans* (Ecsedi et al., 2015). We did not test the phenotypic consequences of the other overexpressed *let-7a* 3′ targets that are not known to be involved in the heterochronic pathway.

It is curious that the mutation of g18, which is one of two 3′ nucleotides of *let-7a* that shows the greatest evolutionary conservation, did not cause visible phenotypes. By ribosome profiling, we found 3 genes that were upregulated in the *let-7a* g18 mutant and that contain 3′ UTR sites with 3′ complementarity, including g18, suggesting that they could be *let-7a* targets whose proper repression depends on g18 pairing. However, caution is called for in interpreting these genes as g18 targets because their Wormbase annotations indicate that in the WT, these transcripts undergo developmental upregulation at the L4 (Harris et al., 2020), which is the stage at which our samples were collected. Thus, based on the Wormbase annotations, the increased RPF observed for these candidate g18 targets in the g18 mutant could be an artifact of slight differences in staging between samples. However, published data from translational profiling of *C. elegans* larvae (Aeschimann et al., 2017) argue against the above caveat, as they show that the translational levels of our candidate g18 targets were not significantly increased from L3 to L4 (Figure S3E). Moreover, in the g18 mutant, 2 of the putative target genes (*chs-1* and *try-1*) were translationally de-repressed without significant difference in mRNA levels (Figures S3B and S3C), suggesting that in these cases, staging differences between samples are unlikely to explain the data. We thus propose that 3′ pairing to *let-7a* at g18 may contribute a dampening of the increase in the translational output of these developmentally upregulated mRNAs. Interestingly, in the Aeschimann et al. (2017) dataset, these putative g18 targets were not translationally de-repressed in *let-7a(n2853, G5C)* (Figure S3F). Although this latter difference with our results could reflect the distinct experimental setups, it is also possible that the U18A mutation may be more detrimental to the proper repression of these putative targets than the G5C seed mutation.

The evolutionary conservation of the *let-7a* sequence

The entire *let-7a* sequence is almost perfectly conserved across bilaterian phyla (Figure 1) (Wolter et al., 2017), suggesting pervasive involvement of *let-7a* in interactions that constrain the g9–g22 sequence. The conservation of g11–g16 of *let-7a* could be driven by phenocritical roles for these nucleotides in the repression of conserved targets and reinforced by a multiplicity of targets with g11–g16 pairing (John et al., 2004), supported by our identifying multiple *C. elegans let-7a* targets with critical non-seed pairing.

Our data do not appreciably illuminate potential mechanisms for the conservation of *let-7a* 3′ distal nucleotides (g17–g22) or the bridge nucleotides (g9–g10). However, although single-nucleotide or compound mutations were phenotypically tolerated in g17–g22, we observed the phenotypic effects of a g18 mutation in the context of a g16 mutation, suggesting the involvement of 3′ distal nucleotides in repressing targets with obligate mismatches to g14–g16 to *let-7a*. It is also possible that *let-7a* 3′ distal nucleotides could interact with miRISC-associated RNA-binding proteins, which recognize specific sequences. Our finding that mutations at g9–g10 were also phenotypically tolerated is consistent with

the observation that *let-7a* is not predicted to engage in target recognition involving g9–g10 paring in *C. elegans*, and that fully complementary target sites that involve the bridge pairing are rare in vertebrates (Bartel, 2018). Interestingly, miRNA bridge nucleotides (g9-g10 for *let-7a*) can be exposed on the miRISC surface even when their sequences are complementary to the target (Sheu-Gruttadauria et al., 2019), suggesting that these nucleotides could engage in interactions external to AGO. We hypothesize that g9–g10 of *let-7a* may be constrained by association with conserved RNA-binding proteins that recognize these nucleotides, possibly in the context of *let-7a* biogenesis or target binding.

It is also possible that the identity of g9–g10 or g17–g22 nucleotides of *let-7a* could be critical for target repression under conditions not assayed in this study, such as various conditions of stress, and/or could be required for target interactions unrelated to the phenotypes that we monitored. The latter possibility is supported by our finding that the g18 mutant displays molecular phenotypes by Ribo-seq and RNA-seq (Figure S3). Such molecular phenotyping of other distal 3′ nucleotides of *let-7a*, and other "silent" nucleotides of other miRNAs, could reveal otherwise experimentally inaccessible functionalities.

Limitations of the study

There are limitations to the use of ribosome profiling of whole animals for the confirmation of *in vivo* miRNA targeting. In particular, the data could contain numerous false negatives, especially for genes that are broadly expressed but are only repressed by miRNAs in specific tissues or cells. For example, although we identified 8 target genes with 3′ non-seed complementarity that were upregulated in the *let-7a* g13 mutant, genes with such 3′ complementarity as a class were not statistically enriched (Figure S6E). Similarly, potential *let-7a* target genes with g18 pairing were also not statistically enriched among the de-repressed genes in the *let-7a* g18 mutant (data not shown; Figure S3).

STAR★METHODS

RESOURCE AVAILABILITY

Lead contact—Further information and request for resources and reagents should be directed to and will be fulfilled by the lead contact Victor Ambros (victor.ambros@umassmed.edu).

Materials availability—All *C. elegans* strains and reagents will be shared upon request. Data and Code Availability The raw and processed data of ribosome profiling, RNA-seq, and small RNA seq in this study have been deposited at NCBI Gene Expression Omnibus (GEO) with accession number GSE171748 (Edgar et al., 2002) and are publicly available. All original code has been deposited at GitHub (https://github.com/IsanaVekslerLublinsky/Let7_Proj_code.git.) with Zenodo DOI 6465945, and is publicly available. Any additional information required to reanalyze the data reported in this paper is available from the lead contact upon request.

Data and code availability

- The raw and processed data of ribosome profiling, RNA-seq, and small RNA seq in this study have been deposited at NCBI Gene Expression Omnibus (GEO) with accession number GSE171748 (Edgar et al., 2002) and are publicly available.
- All original code has been deposited at GitHub (https://github.com/IsanaVekslerLublinsky/Let7_Proj_code.git.) with Zenodo DOI 6465945, and is publicly available.
- Any additional information required to reanalyze the data reported in this paper is available from the lead contact upon request.

EXPERIMENTAL MODEL AND SUBJECT DETAILS

Experimental models: organisms/strains—The genotypes, resources and identifiers (strain names) of the *C. elegans* strains used and the genetic alleles generated in this study are described in Table S5.

METHOD DETAILS

Phylogeny and conservation analysis—Precursor and mature miRNA sequences, and a phylogenetic tree of metazoan species were downloaded from miRbase (v22.1) (Kozomara et al., 2019). An in-house code was developed to identify miRNAs that belong to the *let-7 family* based on the presence of the seed sequence “GAGGUA” at g2-g7 on the mature miRNA. For each species in the collection, the number of total miRNA loci and the number of *let-7* miRNA loci were counted. To calculate the distance of each member to the conserved *hsa-let-7a*, its sequence was aligned to the *hsa-let-7a* sequence and the number of mismatches in the alignment was counted. The phylogenetic trees were visualized with the program evolView v2 (He et al., 2016).

117 species encode *let-7a* family isoforms. From each species, the sequence of one, the most similar to *let-7a*, was extracted and used to construct a conservation profile. A similar analysis was done with the *mir-1* and *mir-34* families to obtain their conservation profiles.

Targeted mutagenesis at the *let-7a* genomic locus—CRISPR/Cas9 genome editing of the *let-7a* locus was performed using the “jump board” strategy previously described (Duan et al., 2020a) on strain *VT3742*, which carries the *let-7(ma393)* insertion of the “jump board” sequence in place of the *pre-let-7* sequence, as well as the genetic balancer *umnIs25(mnDp1)* and a transgene *oxSi1091* expressing Cas9. Templates for dsDNA HR donors were prepared by cloning the WT *pre-let-7a* and 500 bp of flanking sequence into pCR2.1-TOPO vector. The Q5 mutagenesis kit (NEB, Cat: E0554) was used to generate the mutant plasmids. Double-strand DNA donors were generated from the mutant plasmids by PCR with 73/106 base-pairs flanking the *pre-let-7a*, and the PCR product was purified by ethanol precipitation. Injection mixtures containing final concentrations of 30 ng/μL AltR_Cas-9_crRNA_INPP4A_1/2 each, 10 ng/μL AltR_Cas-9 _crRNA_dpy-10_cn64 as co-CRISPR marker (Arribere et al., 2014), 75 ng/μL Alt-R tracrRNA (IDT, Cat:1072532), 10 ng/μL each dsDNA donor in 1X duplex buffer (IDT, Cat: 11010301) were injected into

the gonad of *VT3742* at young adult stage. F1 dumpy animals were isolated and genotyped by PCR with let-7_SEQ_F5/R5 primers followed by an analysis of the PCR product using restriction digestion using EcoRV (NEB, Cat: N3195) and Sanger sequencing as described in Duan et al., (2020a). Mutants were backcrossed with *N2* (for strains without *maIs105*) or *VT1367*(for strains with *maIs105*) for at least two generations.

Targeted mutagenesis at the *lin-41* genomic locus—Ultramer single-strand DNA donors (lengths ranging from 115 nt to 117 nt) with 35 nt flanking homology were obtained from IDT. The injection mixture containing final concentrations of 25 ng/μL AltR_Cas-9_crRNA_lin-41_1/2 each, 15 ng/μL AltR_Cas-9_crRNA_dpy-10_cn64, 95 ng/μL Alt-R tracrRNA (IDT, Cat:1072532), 325 ng/μL each ssDNA donor in 1X duplex buffer (IDT, Cat: 11010301) were incubated at room temperature for 10 min for pre-annealing and injected into the gonad of *EG9615, VT3867* or *VT3873* which contain transgene *oxSi1091* expressing Cas9. F1 dumpy animals were isolated and genotyped by PCR with lin-41_SEQ_F2/R2 primers, followed by an analysis of the PCR product using Sanger sequencing. Mutants were backcrossed with N2 for at least two generations.

Targeted mutagenesis at the *daf-12* genomic locus—Double-stranded DNA donor (length 641 bp) containing the desired mutations plus 65/78 bp flanking homology was obtained from GENEWIZ. The injection mixture, containing final concentrations of 80 ng/μL AltR_Cas-9_crRNA_daf-12_4, 40 ng/μL AltR_Cas-9_crRNA_dpy-10_cn64, 223.3 ng/μL Alt-R tracrRNA (IDT, Cat:1072532), and 73.3 ng/μL dsDNA donor in 1X duplex buffer (IDT, Cat: 11010301), was incubated at room temperature for 10 min for pre-annealing and injected into the gonad of *VT4126* which contain *daf-12(ma498ma567, mScarlet* with 3′ UTR InDel) as a *daf-12* "jump board" and transgene *oxSi1091* expressing Cas9 (Ilbay and Ambros, 2019). Genotyping and backcrossing were performed the same as the *lin-41* locus.

Worm culturing and synchronization—*C.elegans* were cultured on nematode growth medium (NGM) and fed with *E. coli* HB101 unless specified. To obtain populations of synchronized developing worms, gravid adults were collected and washed twice with water. Pellets of centrifuged worms were treated with 5 mL 1 M NaOH and 1% (v/v) sodium hypochlorite for 5 min with shaking to obtain embryos, and the embryos were rinsed with M9 buffer three times. The embryos were hatched in 10 mL M9 buffer at 20°C for 16-18 h with mild shaking. Hatched L1 larvae were transferred to plates at 30-50 worms per plate and replicate plates were cultured at 15°C, 20°C, or 25°C for defined periods; samples of the population were examined by microscopy to confirm the developmental stage at the time of harvest.

Phenotypic assays for vulva defects—The adult lethality characteristic of *let-7(lf)*, which results from rupture of the young adult animal at the vulva, was scored approximately 36 h (15°C), 24 h (20°C) or 16 h (25°C) after the animals reached developmental maturation (when at least 90% of the population had reached the adult stage). The young adult (pre-gravid) with vulva bursting phenotypes was distinguished from those without vulva bursting (matricide due to egg-laying defects) based on the visibility of breached intestinal tissues

from the ruptured vulva region. To score viable progeny per adult, young adults were transferred to a fresh plate every 12 h until those capable of laying eggs had completed egg-laying. Only hatched eggs were counted.

Microscopy and heterochronic phenotypes—Differential interference contrast and fluorescent images were obtained by Zeiss.Z1 equipped with ZEISS Axiocam 503 camera. COL-19::GFP pattern images of the whole animal were obtained using a 10X objective. Adult alae and GFP::LIN-41 images were obtained using a 100X objective. DAF-12::mScarlet images were obtained using a 63X objective. Lateral hypodermal heterochronic cell lineage defects were scored by counting the number of seam cells per side of each animal with the aid of the *wIs51* transgenic seam cell reporter. Patterns of expression of the adult-specific COL-19::GFP reporter were scored using the *maIs105* transgenic reporter. Fluorescent images were processed by ImageJ FIJI (Schindelin et al., 2012). To quantify the DAF-12::mScarlet expression, total fluorescence signal and area of individual seam cell and Hyp7 nuclei were quantified by ImageJ FIJI, and the fluorescence signal density of one posterior and one anterior region adjacent to each nucleus was measured and used to calculate the background signal for that nucleus. The choice of conventional epifluorescence microscopy was motivated by the limitation that DIC optics was required to locate each nucleus before fluorescence illumination and that a confocal microscope with DIC capability was not available. The underlying constraint in the cases of DAF-12::mSCARLET and LIN-41::GFP is that the signals exhibit strong photobleaching, so it was necessary to initiate fluorescence image acquisition simultaneously with turning on the UV illumination, and only after having used DIC white light microscopy to identify the seam and Hyp7 nuclei at the appropriate focal plane. The photobleaching issue also prompted us to choose the cautious limit of one exposure per animal.

RNAi—Overnight cultures of HT115 bacteria expressing dsRNA (Timmons et al., 2001) were transferred to LB broth and shaken at 37°C until OD_{600} was between 0.4 – 0.8. The bacteria cultures were spread on NGM medium containing 100 μg/mL ampicillin and 1 mM IPTG and induced at room temperature for 24-48 h. HT115 bacteria strains for RNAi were obtained from the Ahringer library (Kamath et al., 2003).

Total RNA preparation—Harvested worms were washed with M9 medium, centrifuged, and the worm pellets were flash-frozen in liquid nitrogen. The worm pellets were thawed and lysed by adding 4X volumes of QIAzol (Qiagen, Cat: 79306) and shaking vigorously at room temperature for 15 min. The total RNA was extracted by the addition of 0.85X volume chloroform, centrifugation, and recovery of the aqueous phase, which was then re-extracted with 1 volume phenol:chloroform:isoamyl alcohol (25:24:1, pH = 5.5). Total RNA was then precipitated by adding 1 volume of isopropanol and 0.5 μL GlycoBlue (Invitrogen, Cat: AM9516), followed by incubation at −80°C for at least 30 min, and recovery by centrifugation at 25,000 rcf for 10 min at 4°C. The supernatants were then removed, and the RNA pellets were subsequently washed twice by 70% (v/v) ethanol, dried in air for 5 min, dissolved in water, and stored at −80°C.

Fireplex miRNA assay—Synchronized populations of developing worms were cultured at 20°C and harvested at 8 h (L1), 22 h (L2), 36 h (L3), 46 h (L4), and 58 h (adult) after feeding. Total RNA was extracted and miRNA levels of *miR-84* and *let-7a* were quantified by FirePlex miRNA assay (Abcam) with customized *C.elegans* miRNA panel following the manufacturer's instructions. Guava easyCyte 8HT (Millipore) was used for readout. To normalize the quantification, synthetic RNA oligonucleotides with sequences of *miR-84* and *let-7a* (IDT) were serially diluted and subjected to FirePlex miRNA assay. Equal amounts of total RNA were used for all the samples and replicates. The amounts of miRNA in experimental samples were calculated from the standard curve generated from the serial dilution of respective synthetic RNA oligonucleotides. Note that this detection method stringently distinguishes *let-7a* from *miR-84*, as *let-7a* was not detected in *let-7(ma341)* and *miR-84* was not detected in *mir-84(n4037)* (Figures 2C-2D).

qRT-PCR analysis—20–25 synchronized worms were cultured at 25°C and harvested at the mid-L4 stage (30 h after feeding). Total RNA was extracted as described above. Reverse transcription was performed using HiFiScript gDNA Removal RT MasterMix (CWBio, Cat: CW2020M) with 100 ng total RNA input. qPCR was performed using UltraSYBR Mixture (CWBio, Cat: CW2601) on ViiA 7 platform.

Small RNA sequencing—Synchronized populations of developing worms were cultured at 20°C and harvested at the mid-late L4 stage (45 h after feeding). Total RNA was extracted as described above. The small RNA sequencing libraries were constructed using NEBNext multiplex small RNA library prep set (NEB, Cat: E7300), and sequenced by Illumina NextSeq 500 system. The adaptor sequences were trimmed from the 3′ end of the raw reads by *Cutadapt/1.9* using default parameters (Martin, 2011). To quantify the wild type or mutant *let-7a* miRNAs, the trimmed reads were mapped with *Bowtie2/2.3.4.3* to either wild type or mutant *let-7a* sequences indexed with *-c* using parameters *-end-to-end -N 0 -no-1mm-upfront -L 22* (Langmead and Salzberg, 2012). To quantify the total small RNA reads, trimmed reads were size filtered by *Cutadapt/1.9*, and reads with a length between 18-25 bp were kept. The filtered reads were mapped to *C. elegans* genome *WBCel235* by *star/2.7.6a* with default parameters (Dobin et al., 2013). The numbers of reads that mapped uniquely to the genome were used to calculate the RPM of wild type and mutant *let-7a*. Gene counting was done by *subread1.6.2/featureCounts* (Liao et al., 2014). The total number of miRNA reads that mapped uniquely to the genome were used to calculate the RPMs of wild type and mutant *let-7a*.

Ribosome profiling

Worm harvesting: Synchronized populations of developing worms were cultured at 20°C for 45 h after feeding. Harvested worms were harvested by M9, washed with water three times, and incubated at room temperature for 10 min to allow digestion of intestinal bacteria. Worms were then pelleted by centrifuge at 4,500 rcf for 2 min at room temperature and residual water was removed until the total volumes were twice as the worm pellets. The samples were then flashed frozen by liquid nitrogen and stored at −80°C.

Monosome preparation: Concentrated lysis buffer was added to each frozen sample to a final concentration of 20 mM Tris-HCl (pH = 7.4), 150 mM NaCl, 5mM $MgCl_2$, 0.5X Protease Inhibitor (Sigma, Cat:P2714), 1 mM DTT, 0.1 mg/mL cycloheximide (Millipore, Cat:C4859), 1% (v/v) Triton X-100 and 5 U/mL Turbo DNase (Invitrogen, Cat:AM2238) (Ingolia et al., 2012), and worm pellets were kept on ice until fully thawed. Suspended worms were transferred to 400 μm silica beads tube (OPS Diagnostic, Cat: PFAW-400-100-04) and lysed in bead beater homogenizer for 4 min at 4°C. Lysates were then centrifuged at 25,000 rcf for 10 min at 4°C, and supernatants were collected. To generate monosomes, RNase I (Invitrogen, Cat: AM2294) was added to a final concentration of 0.2 U per μl of harvested worm pellet. The digestion was incubated at room temperature for 40 min with gentle rotation and then quenched by adding SUPERase RNase inhibitor (Invitrogen, Cat: AM2694) at 4 U per RNase I unit. The lysates were then loaded onto 5-40% (m/v) sucrose gradients prepared with lysis buffer without Triton X-100 and centrifuged at 32,000 rpm for 3 h at 4°C in an SW41Ti rotor (Beckman Coulter, Cat:331362). The sucrose gradients were fractionated using BR-188 Density Gradient Fractionation System with 60% (m/v) sucrose as chase solution, and monosome fractions were collected according to OD_{254} profiles.

RPF cloning: 3.5 X volumes of QIAzol reagent were added to the gradient fractions containing monosomes, and RNA was extracted and separated by 17.5% denaturing PAGE. A synthetic RNA oligonucleotide with a length of 30 nt was used as a size marker. The gel was stained by Sybr Gold (Invitrogen, Cat: S11494) at room temperature for 10 min, and a gel slice containing RNA of approximately 30 nt was excised and ground by an RNase-free pellet pestle (Fisher Scientific, Cat: 12-141-364). RNA was extracted from the gel slice by adding 500 μL of 300 mM NaAc (pH = 5.5), 1 mM EDTA, and 0.25% (m/v) SDS and mildly shaking overnight at room temperature (Ingolia et al., 2012). The gel granules were excluded using Spin-X tube filter (Millipore, Cat: CLS8160) and the RNA was then concentrated by ethanol precipitation, dissolved in water, and stored at −80°C. 5′ phosphorylation and 3′ dephosphorylation were performed with T4 PNK (NEB, Cat: M0201S) following the manufacturer's instructions, and the products were subjected to phenol/chloroform extraction and ethanol precipitation. cDNA libraries were constructed using QIAseq miRNA Library Kit (Qiagen, Cat:331505 & 331595) following the manufacturer's instructions, except that the amplifying PCR was conducted with 9-12 cycles, and sequencing was performed using Illumina NextSeq 500 system.

RPF data analysis: The adaptor sequences were trimmed from the 3′ end of the raw reads by the *Cutadapt/1.9* using default parameters (Martin, 2011). Reads were size filtered to keep only reads with a length between 26-34 bp (a range that fits ribosome-protected fragments) (Aeschimann et al., 2015). The rRNA and tRNA reads were removed by initially mapping with *Bowtie2/2.3.4.3* to *C. elegans* rRNA and tRNA sequences from *WBCel235* with default parameters (Chan and Lowe, 2009, 2016; Langmead and Salzberg, 2012), and the remaining reads were mapped to the *C. elegans* genome *WBcel235* by *Star/2.5.3* with default parameters. The p-offset of the 5′ end of the mapped reads and the monosome periodicity were determined by *plastid/0.4.8* as quality control, and gene counting on exons was generated by *plastid_cs/0.4.8* with p-offset adjusted (Dunn and Weissman, 2016;

Santos et al., 2019). Differential expression analysis was performed by *DESeq2* with default parameters (Kucukural et al., 2019; Love et al., 2014). Genes with a max raw count smaller than 10 were excluded from the analysis. Volcano plots were generated using *ggplot2* (Hadley, 2016).

To identify genes whose observed expression perturbation between mutant and wild-type samples could be due to slight differences in staging between sample populations, the gene expression changes between the mutants and wild-type were compared with the expression changes between different developmental time points published previously (Aeschimann et al., 2019). Of particular interest were genes reported to change in N2 between 28 and 30 h, and/or between 30 and 32 h at 25°C (Aeschimann et al., 2017), which corresponds to the L4 harvest time point at 20°C used in this study. A gene was flagged as potentially non-specifically perturbed owing to imperfect synchrony if the normalized RPF fold change that we observed between mutant and wild-type was smaller than 1.5 times of the reported RPF fold change between two developmental time points in the wild-type (Aeschimann et al., 2017).

RNAseq of mRNA after ribosomal RNA depletion—To ensure mRNA representation in our samples regardless of poly(A) status we enriched for mRNA in our samples using ribosomal RNA depletion with rRNA anti-sense oligos and RNaseH (Duan et al., 2020b). Worm samples for RNA-seq were aliquoted from the ribosome profiling harvests before the lysis step and frozen separately. The total RNA was extracted as described above. To enrich for mRNA, rRNA was depleted as described in Duan et al., (2020b). rRNA-depleted mRNA samples were then purified by RNA Clean & Concentrator-5 Kit (ZYMO, Cat: R1015) (Zhang et al., 2012). The RNA-seq libraries were constructed by NEBNext Ultra II RNA Library Prep kit (NEB, Cat: E7775, E7335, E7500) and sequenced by Illumina NextSeq 500 system (Duan et al., 2020b).

RNA-seq and translational efficiency data analysis—The adaptor sequences were trimmed from RNA-seq data and reads shorter than 15 nt were filtered out from the analysis by *Cutadapt/1.9*. tRNA, signal recognition particle RNA (srpR), and residual cytoplasmic rRNA reads were removed by initial mapping with *Bowtie2/2.3.4.3*, and the remaining reads were mapped to *C. elegans* genome *WBcel235* by *Star/2.5.3* with default parameters. Gene counting was done by *featureCounts(Subread/1.6.2)* (Liao et al., 2014). Differential expression analysis was performed by *DESeq2* with default settings (Kucukural et al., 2019; Love et al., 2014). To calculate the translational efficiency (TE), the genes with a max raw count smaller than 10 for either RNA-seq or ribosome profiling were excluded from the analysis. The TE was calculated by dividing normalized ribosome profiling counts by normalized RNA-seq counts for each replica. Significance was calculated by the Student t-test. Volcano plots were generated using *ggplot2*.

Target prediction—3′ UTR sequences of C. elegans genes were downloaded from the WormBase Parasite website (Howe et al., 2016, 2017) for the genomic version *WBcel235*. The UTRs were sorted and filtered to remove redundant sequences. The final dataset contained 15,058 3′UTR sequences for 13975 genes (some genes have more than one 3′UTR isoform). The target sites of *let-7a* sequence that obey one of the following criteria

were predicted using the algorithm developed in Veksler-Lublinsky et al., (2010): (1) perfect Watson-Crick (W/C) complementarity (perfect match) to positions 2-7; (2) W/C match to positions 2-7, but allowing 1 target bulge in positions 5-7; (3) W/C match to positions 2-8, but allowing 1 GU/Mismatch (MM) in positions 5-8; (4) W/C match to positions 2-7, but allowing 1 mRNA bulge in positions 2-4; (5) W/C match to positions 2-8, but allowing 1 GU/MM in positions 2-4.

For sites that obey one of the above criteria, a flanking region of an additional 20 nt after the seed was extracted. The interaction duplex between the full site and the miRNA was then calculated using RNAduplex (Lorenz et al., 2011). The duplex was parsed to identify both the seed type and the non-seed type for each reported interaction as follows: (A) **Seed type**: "1" 2-7 full match; "2" 2-7 + 1 target bulge on 5-7 or 2-8 with 1GU/MM 5-8; "3" 2-7 + 1 target bulge on 2-4 or 2-8 with 1 GU/MM 2-4. (B) **NonSeed type**: "1" perfect match to positions 11-13 or 12-14 or 13-16; "2" match allowing GUs to positions 11-13 or 12-14 or 13-16; "−1" none of the above. Note that our unpublished data suggest that a single GU in 3′ non-seed region may not significantly affect miRNA repressing efficacy. For genes that have multiple UTR sequences in the analysis, UTRs with redundant duplexes were filtered out from the final report.

In the output results (Table S4 and Data S1), site configurations are categorized in (SeedType, NonSeedType) format. For SeedType, '1' indicates sites with g2-g7 perfect seed pairing; '2' indicates sites with mildly imperfect seed pairing (1 GU/mismatch at g5-g8 or 1 target nucleotide bulge at t5-t7); '3′ indicates sites with severely imperfect seed pairing (1 GU/mismatch at g2-g4 or 1 target nucleotide bulge at t2-t4). For NonSeedType, '1' indicates sites with at least 3 consecutive Watson-Crick pairing to g11-g16 of *let-7a* (g13 must be pairing); '2' indicates sites with at least 3 consecutive pairing to g11-g16 of *let-7a* with GU wobble (g13 must be pairing); '−1' indicates other sites which are considered as no critical non-seed pairing.

QUANTIFICATION AND STATISTICAL ANALYSIS

In Figure 5A, *DEseq2* was used for differential expression analysis of ribosome occupancy, significantly perturbed genes were defined by FC > 1.5 and p.adj <0.1 by *DEseq2*. In Figure 5C, *DEseq2* was used for differential expression analysis of mRNA abundance, genes with significantly increased mRNA abundance were defined by FC > 1.5, p.adj <0.1 by *DESeq2;* Student's t test was used for differential expression analysis of TE, genes with significantly increased TE were defined by FC > 1.5, p < 0.1 by Student's t test. In Figures 2G, 3C, 4F, 5F, 6A-6H, and 7B, the p-values representation is as follow: 0.05–0.01(*); 0.01–0.001(**); 0.001–0.0001(***); <0.0001(****) by Student's t test (two-tailed, unpaired). Error bars indicate mean ± SD. Significance tests were conducted with Prism 8. Statistical details can be found in corresponding figure legends.

Supplementary Material

Refer to Web version on PubMed Central for supplementary material.

ACKNOWLEDGMENTS

We thank Xantha Karp, Charles Nelson, and Alejandro Vasquez-Rifo for commenting on the manuscript. This research was supported by funding from NIH grants R01GM088365, R01GM034028, and R35GM131741 (to V.A.). Some *C. elegans* strains were provided by the CGC, which is funded by the NIH Office of Research Infrastructure Programs (P40 OD010440).

REFERENCES

Abbott AL, Alvarez-Saavedra E, Miska EA, Lau NC, Bartel DP, Horvitz HR, and Ambros V (2005). The let-7 MicroRNA family members mir-48, mir-84, and mir-241 function together to regulate developmental timing in Caenorhabditis elegans. Dev. Cell 9, 403–414. [PubMed: 16139228]

Abrahante JE, Daul AL, Li M, Volk ML, Tennessen JM, Miller EA, and Rougvie AE (2003). The Caenorhabditis elegans hunchback-like gene lin-57/hbl-1 controls developmental time and is regulated by microRNAs. Dev. Cell 4, 625–637. [PubMed: 12737799]

Aeschimann F, Kumari P, Bartake H, Gaidatzis D, Xu L, Ciosk R, and Grosshans H (2017). LIN41 post-transcriptionally silences mRNAs by two distinct and position-dependent mechanisms. Mol. Cell 65, 476–489.e4. [PubMed: 28111013]

Aeschimann F, Neagu A, Rausch M, and Grosshans H (2019). let-7 coordinates the transition to adulthood through a single primary and four secondary targets. Life Sci. Alliance 2, e201900335. [PubMed: 30910805]

Aeschimann F, Xiong J, Arnold A, Dieterich C, and Grosshans H (2015). Transcriptome-wide measurement of ribosomal occupancy by ribosome profiling. Methods 85, 75–89. [PubMed: 26102273]

Alvarez-Saavedra E, and Horvitz HR (2010). Many families of C. elegans microRNAs are not essential for development or viability. Curr. Biol 20, 367–373. [PubMed: 20096582]

Ambros V (2004). The functions of animal microRNAs. Nature 431, 350–355. [PubMed: 15372042]

Arribere JA, Bell RT, Fu BX, Artiles KL, Hartman PS, and Fire AZ (2014). Efficient marker-free recovery of custom genetic modifications with CRISPR/Cas9 in Caenorhabditis elegans. Genetics 198, 837–846. [PubMed: 25161212]

Bagga S, Bracht J, Hunter S, Massirer K, Holtz J, Eachus R, and Pasquinelli AE (2005). Regulation by let-7 and lin-4 miRNAs results in target mRNA degradation. Cell 122, 553–563. [PubMed: 16122423]

Balzeau J, Menezes MR, Cao S, and Hagan JP (2017). The LIN28/let-7 pathway in cancer. Front. Genet 8, 31. [PubMed: 28400788]

Bartel DP (2018). Metazoan MicroRNAs. Cell 173, 20–51. [PubMed: 29570994]

Bazzini AA, Lee MT, and Giraldez AJ (2012). Ribosome profiling shows that miR-430 reduces translation before causing mRNA decay in zebrafish. Science 336, 233–237. [PubMed: 22422859]

Brancati G, and Grosshans H (2018). An interplay of miRNA abundance and target site architecture determines miRNA activity and specificity. Nucleic Acids Res. 46, 3259–3269. [PubMed: 29897601]

Brennecke J, Stark A, Russell RB, and Cohen SM (2005). Principles of microRNA-target recognition. PLoS Biol. 3, e85. [PubMed: 15723116]

Brenner JL, Kemp BJ, and Abbott AL (2012). The mir-51 family of microRNAs functions in diverse regulatory pathways in Caenorhabditis elegans. PLoS One 7, e37185. [PubMed: 22615936]

Broughton JP, Lovci MT, Huang JL, Yeo GW, and Pasquinelli AE (2016). Pairing beyond the seed supports MicroRNA targeting specificity. Mol. Cell 64, 320–333. [PubMed: 27720646]

Chan PP, and Lowe TM (2009). GtRNAdb: a database of transfer RNA genes detected in genomic sequence. Nucleic Acids Res. 37, D93–D97. [PubMed: 18984615]

Chan PP, and Lowe TM (2016). GtRNAdb 2.0: an expanded database of transfer RNA genes identified in complete and draft genomes. Nucleic Acids Res. 44, D184–D189. [PubMed: 26673694]

Chi SW, Hannon GJ, and Darnell RB (2012). An alternative mode of microRNA target recognition. Nat. Struct. Mol. Biol 19, 321–327. [PubMed: 22343717]

Denman RB (1993). Using RNAFOLD to predict the activity of small catalytic RNAs. BioTechniques 15, 1090–1095. [PubMed: 8292343]

Dobin A, Davis CA, Schlesinger F, Drenkow J, Zaleski C, Jha S, Batut P, Chaisson M, and Gingeras TR (2013). STAR: ultrafast universal RNA-seq aligner. Bioinformatics 29, 15–21. [PubMed: 23104886]

Doench JG, and Sharp PA (2004). Specificity of microRNA target selection in translational repression. Genes Dev. 18, 504–511. [PubMed: 15014042]

Duan Y, Choi S, Nelson C, and Ambros V (2020a). Engineering essential genes with a "jump board" strategy using CRISPR/Cas9. MicroPubl Biol. 2020. 10.17912/micropub.biology.000315.

Duan Y, Sun Y, and Ambros V (2020b). RNA-seq with RNase H-based ribosomal RNA depletion specifically designed for C. elegans. MicroPubl Biol. 2020. 10.17912/micropub.biology.000312.

Dunn JG, and Weissman JS (2016). Plastid: nucleotide-resolution analysis of next-generation sequencing and genomics data. BMC Genomics 17, 958. [PubMed: 27875984]

Ecsedi M, and Grosshans H (2013). LIN-41/TRIM71: emancipation of a miRNA target. Genes Dev. 27, 581–589. [PubMed: 23512656]

Ecsedi M, Rausch M, and Grosshans H (2015). The let-7 microRNA directs vulval development through a single target. Dev. Cell 32, 335–344. [PubMed: 25669883]

Edgar R, Domrachev M, and Lash AE (2002). Gene Expression Omnibus: NCBI gene expression and hybridization array data repository. Nucleic Acids Res. 30, 207–210. [PubMed: 11752295]

Friedman RC, Farh KK, Burge CB, and Bartel DP (2009). Most mammalian mRNAs are conserved targets of microRNAs. Genome Res. 19, 92–105. [PubMed: 18955434]

Giraldez AJ, Mishima Y, Rihel J, Grocock RJ, Van Dongen S, Inoue K, Enright AJ, and Schier AF (2006). Zebrafish MiR-430 promotes deadenylation and clearance of maternal mRNAs. Science 312, 75–79. [PubMed: 16484454]

Grimson A, Farh KK, Johnston WK, Garrett-Engele P, Lim LP, and Bartel DP (2007). MicroRNA targeting specificity in mammals: determinants beyond seed pairing. Mol. Cell 27, 91–105. [PubMed: 17612493]

Grosshans H, Johnson T, Reinert KL, Gerstein M, and Slack FJ (2005). The temporal patterning microRNA let-7 regulates several transcription factors at the larval to adult transition in C. elegans. Dev. Cell 8, 321–330. [PubMed: 15737928]

Grosswendt S, Filipchyk A, Manzano M, Klironomos F, Schilling M, Herzog M, Gottwein E, and Rajewsky N (2014). Unambiguous identification of miRNA:target site interactions by different types of ligation reactions. Mol. Cell 54, 1042–1054. [PubMed: 24857550]

Hadley W (2016). Ggplot2 (Springer Science+Business Media, LLC).

Hammell CM, Karp X, and Ambros V (2009). A feedback circuit involving let-7-family miRNAs and DAF-12 integrates environmental signals and developmental timing in Caenorhabditis elegans. Proc. Natl. Acad. Sci. U S A 106, 18668–18673. [PubMed: 19828440]

Harris TW, Arnaboldi V, Cain S, Chan J, Chen WJ, Cho J, Davis P, Gao S, Grove CA, Kishore R, et al. (2020). WormBase: a modern model organism information resource. Nucleic Acids Res. 48, D762–D767. [PubMed: 31642470]

He Z, Zhang H, Gao S, Lercher MJ, Chen WH, and Hu S (2016). Evolview v2: an online visualization and management tool for customized and annotated phylogenetic trees. Nucleic Acids Res. 44, W236–W241. [PubMed: 27131786]

Helwak A, Kudla G, Dudnakova T, and Tollervey D (2013). Mapping the human miRNA interactome by CLASH reveals frequent noncanonical binding. Cell 153, 654–665. [PubMed: 23622248]

Hertel J, Bartschat S, Wintsche A, Otto C, and The Students of the Bioinformatics Computer, Lab; and Stadler PF (2012). Evolution of the let-7 microRNA family. RNA Biol. 9, 231–241. [PubMed: 22617875]

Howe KL, Bolt BJ, Cain S, Chan J, Chen WJ, Davis P, Done J, Down T, Gao S, Grove C, et al. (2016). WormBase 2016: expanding to enable helminth genomic research. Nucleic Acids Res. 44, D774–D780. [PubMed: 26578572]

Howe KL, Bolt BJ, Shafie M, Kersey P, and Berriman M (2017). WormBase ParaSite - a comprehensive resource for helminth genomics. Mol. Biochem. Parasitol. 215, 2–10. [PubMed: 27899279]

Ilbay O, and Ambros V (2019). Regulation of nuclear-cytoplasmic partitioning by the lin-28-lin-46 pathway reinforces microRNA repression of HBL-1 to confer robust cell-fate progression in C. elegans. Development 146, dev183111. [PubMed: 31597658]

Ingolia NT (2016). Ribosome footprint profiling of translation throughout the genome. Cell 165, 22–33. [PubMed: 27015305]

Ingolia NT, Brar GA, Rouskin S, McGeachy AM, and Weissman JS (2012). The ribosome profiling strategy for monitoring translation in vivo by deep sequencing of ribosome-protected mRNA fragments. Nat. Protoc 7, 1534–1550. [PubMed: 22836135]

John B, Enright AJ, Aravin A, Tuschl T, Sander C, and Marks DS (2004). Human MicroRNA targets. PLoS Biol. 2, e363. [PubMed: 15502875]

Kamath RS, Fraser AG, Dong Y, Poulin G, Durbin R, Gotta M, Kanapin A, Le Bot N, Moreno S, Sohrmann M, et al. (2003). Systematic functional analysis of the Caenorhabditis elegans genome using RNAi. Nature 421, 231–237. [PubMed: 12529635]

Kozomara A, Birgaoanu M, and Griffiths-Jones S (2019). miRBase: from microRNA sequences to function. Nucleic Acids Res. 47, D155–D162. [PubMed: 30423142]

Kucukural A, Yukselen O, Ozata DM, Moore MJ, and Garber M (2019). DEBrowser: interactive differential expression analysis and visualization tool for count data. BMC Genomics 20, 6. [PubMed: 30611200]

Lai EC (2002). Micro RNAs are complementary to 3′ UTR sequence motifs that mediate negative post-transcriptional regulation. Nat. Genet 30, 363–364. [PubMed: 11896390]

Langmead B, and Salzberg SL (2012). Fast gapped-read alignment with Bowtie 2. Nat. Methods 9, 357–359. [PubMed: 22388286]

Lee H, Han S, Kwon CS, and Lee D (2016). Biogenesis and regulation of the let-7 miRNAs and their functional implications. Protein Cell 7, 100–113. [PubMed: 26399619]

Lee RC, Feinbaum RL, and Ambros V (1993). The C. elegans heterochronic gene lin-4 encodes small RNAs with antisense complementarity to lin-14. Cell 75, 843–854. [PubMed: 8252621]

Lewis BP, Burge CB, and Bartel DP (2005). Conserved seed pairing, often flanked by adenosines, indicates that thousands of human genes are microRNA targets. Cell 120, 15–20. [PubMed: 15652477]

Liao Y, Smyth GK, and Shi W (2014). featureCounts: an efficient general purpose program for assigning sequence reads to genomic features. Bioinformatics 30, 923–930. [PubMed: 24227677]

Lim LP, Lau NC, Garrett-Engele P, Grimson A, Schelter JM, Castle J, Bartel DP, Linsley PS, and Johnson JM (2005). Microarray analysis shows that some microRNAs downregulate large numbers of target mRNAs. Nature 433, 769–773. [PubMed: 15685193]

Liu Z, Kirch S, and Ambros V (1995). The Caenorhabditis elegans heterochronic gene pathway controls stage-specific transcription of collagen genes. Development 121, 2471–2478. [PubMed: 7671811]

Lorenz R, Bernhart SH, Honer Zu Siederdissen C, Tafer H, Flamm C, Stadler PF, and Hofacker IL (2011). ViennaRNA package 2.0. Algorithms Mol. Biol 6, 26. [PubMed: 22115189]

Love MI, Huber W, and Anders S (2014). Moderated estimation of fold change and dispersion for RNA-seq data with DESeq2. Genome Biol. 15, 550. [PubMed: 25516281]

Martin M (2011). Cutadapt removes adapter sequences from high-throughput sequencing reads. EMB J. 17, 3.

McGeary SE, Bisaria N, Pham TM, Wang PY, and Bartel DP (2022). MicroRNA 3′-compensatory pairing occurs through two binding modes, with affinity shaped by nucleotide identity and position. Elife 11.

Nelson C, and Ambros V (2019). Trans-splicing of the C. elegans let-7 primary transcript developmentally regulates let-7 microRNA biogenesis and let-7 family microRNA activity. Development 146, dev172031. [PubMed: 30770392]

Nelson C, and Ambros V (2021). A cohort of Caenorhabditis species lacking the highly conserved let-7 microRNA. G3 11, jkab022. [PubMed: 33890616]

Nottrott S, Simard MJ, and Richter JD (2006). Human let-7a miRNA blocks protein production on actively translating polyribosomes. Nat. Struct. Mol. Biol 13, 1108–1114. [PubMed: 17128272]

Pasquinelli AE, McCoy A, Jimenez E, Salo E, Ruvkun G, Martindale MQ, and Baguna J (2003). Expression of the 22 nucleotide let-7 heterochronic RNA throughout the Metazoa: a role in life history evolution? Evol. Dev 5, 372–378. [PubMed: 12823453]

Paul P, Chakraborty A, Sarkar D, Langthasa M, Rahman M, Bari M, Singha RS, Malakar AK, and Chakraborty S (2018). Interplay between miRNAs and human diseases. J. Cell. Physiol 233, 2007–2018. [PubMed: 28181241]

Pawlica P, Sheu-Gruttadauria J, MacRae IJ, and Steitz JA (2020). How complementary targets expose the microRNA 3′ end for tailing and trimming during target-directed microRNA degradation. Cold Spring Harb. Symp. Quant. Biol 84, 179–183.

Rehmsmeier M, Steffen P, Hochsmann M, and Giegerich R (2004). Fast and effective prediction of microRNA/target duplexes. Rna 10, 1507–1517. [PubMed: 15383676]

Reinhart BJ, Slack FJ, Basson M, Pasquinelli AE, Bettinger JC, Rougvie AE, Horvitz HR, and Ruvkun G (2000). The 21-nucleotide let-7 RNA regulates developmental timing in Caenorhabditis elegans. Nature 403, 901–906. [PubMed: 10706289]

Roush S, and Slack FJ (2008). The let-7 family of microRNAs. Trends Cell Biol. 18, 505–516. [PubMed: 18774294]

Salomon WE, Jolly SM, Moore MJ, Zamore PD, and Serebrov V (2015). Single-molecule imaging reveals that Argonaute reshapes the binding properties of its nucleic acid guides. Cell 162, 84–95. [PubMed: 26140592]

Santos DA, Shi L, Tu BP, and Weissman JS (2019). Cycloheximide can distort measurements of mRNA levels and translation efficiency. Nucleic Acids Res. 47, 4974–4985. [PubMed: 30916348]

Schindelin J, Arganda-Carreras I, Frise E, Kaynig V, Longair M, Pietzsch T, Preibisch S, Rueden C, Saalfeld S, Schmid B, et al. (2012). Fiji: an open-source platform for biological-image analysis. Nat. Methods 9, 676–682. [PubMed: 22743772]

Schirle NT, Sheu-Gruttadauria J, and MacRae IJ (2014). Structural basis for microRNA targeting. Science 346, 608–613. [PubMed: 25359968]

Sheu-Gruttadauria J, Xiao Y, Gebert LF, and MacRae IJ (2019). Beyond the seed: structural basis for supplementary microRNA targeting by human Argonaute2. EMBO J. 38, e101153. [PubMed: 31268608]

Sokol NS, Xu P, Jan YN, and Ambros V (2008). Drosophila let-7 microRNA is required for remodeling of the neuromusculature during metamorphosis. Genes Dev. 22, 1591–1596. [PubMed: 18559475]

Spike CA, Coetzee D, Eichten C, Wang X, Hansen D, and Greenstein D (2014). The TRIM-NHL protein LIN-41 and the OMA RNA-binding proteins antagonistically control the prophase-to-metaphase transition and growth of Caenorhabditis elegans oocytes. Genetics 198, 1535–1558. [PubMed: 25261698]

Sulston JE, Schierenberg E, White JG, and Thomson JN (1983). The embryonic cell lineage of the nematode Caenorhabditis elegans. Dev. Biol 100, 64–119. [PubMed: 6684600]

Tennessen JM, and Thummel CS (2008). Developmental timing: let-7 function conserved through evolution. Curr. Biol 18, R707–R708. [PubMed: 18727906]

Timmons L, Court DL, and Fire A (2001). Ingestion of bacterially expressed dsRNAs can produce specific and potent genetic interference in Caenorhabditis elegans. Gene 263, 103–112. [PubMed: 11223248]

Veksler-Lublinsky I, Shemer-Avni Y, Kedem K, and Ziv-Ukelson M (2010). Gene bi-targeting by viral and human miRNAs. BMC Bioinformatics 11, 249. [PubMed: 20465802]

Vella MC, Choi EY, Lin SY, Reinert K, and Slack FJ (2004). The C. elegans microRNA let-7 binds to imperfect let-7 complementary sites from the lin-41 3′UTR. Genes Dev. 18, 132–137. [PubMed: 14729570]

Wahlquist C, Jeong D, Rojas-Munoz A, Kho C, Lee A, Mitsuyama S, van Mil A, Park WJ, Sluijter JP, Doevendans PA, et al. (2014). Inhibition of miR-25 improves cardiac contractility in the failing heart. Nature 508, 531–535. [PubMed: 24670661]

Waterhouse AM, Procter JB, Martin DM, Clamp M, and Barton GJ (2009). Jalview Version 2–a multiple sequence alignment editor and analysis workbench. Bioinformatics 25 (9), 1189. [PubMed: 19151095]

Wee LM, Flores-Jasso CF, Salomon WE, and Zamore PD (2012). Argonaute divides its RNA guide into domains with distinct functions and RNA-binding properties. Cell 151, 1055–1067. [PubMed: 23178124]

Wolter JM, Le HH, Linse A, Godlove VA, Nguyen TD, Kotagama K, Lynch A, Rawls A, and Mangone M (2017). Evolutionary patterns of metazoan microRNAs reveal targeting principles in the let-7 and miR-10 families. Genome Res. 27, 53–63. [PubMed: 27927717]

Worringer KA, Rand TA, Hayashi Y, Sami S, Takahashi K, Tanabe K, Narita M, Srivastava D, and Yamanaka S (2014). The let-7/LIN-41 pathway regulates reprogramming to human induced pluripotent stem cells by controlling expression of prodifferentiation genes. Cell Stem Cell 14, 40–52. [PubMed: 24239284]

Xiao Y, and MacRae IJ (2020). Robust differential microRNA targeting driven by supplementary interactions in vitro. RNA 26, 162–174. [PubMed: 31732536]

Zhang H, Artiles KL, and Fire AZ (2015). Functional relevance of "seed" and "non-seed" sequences in microRNA-mediated promotion of C. elegans developmental progression. RNA 21, 1980–1992. [PubMed: 26385508]

Zhang Z, Theurkauf WE, Weng Z, and Zamore PD (2012). Strand-specific libraries for high throughput RNA sequencing (RNA-Seq) prepared without poly(A) selection. Silence 3, 9. [PubMed: 23273270]

Highlights

- Single nucleotide at g11–g16 are critical for *in vivo* function of microRNA *let-7a*
- *let-7a* 3′ pairing mediates both perfect and imperfect seed interactions
- A multiplicity of *let-7a* target genes is regulated through 3′ non-seed pairing
- The *let-7a* 3′ sequence cannot be replaced by that of a close family paralog

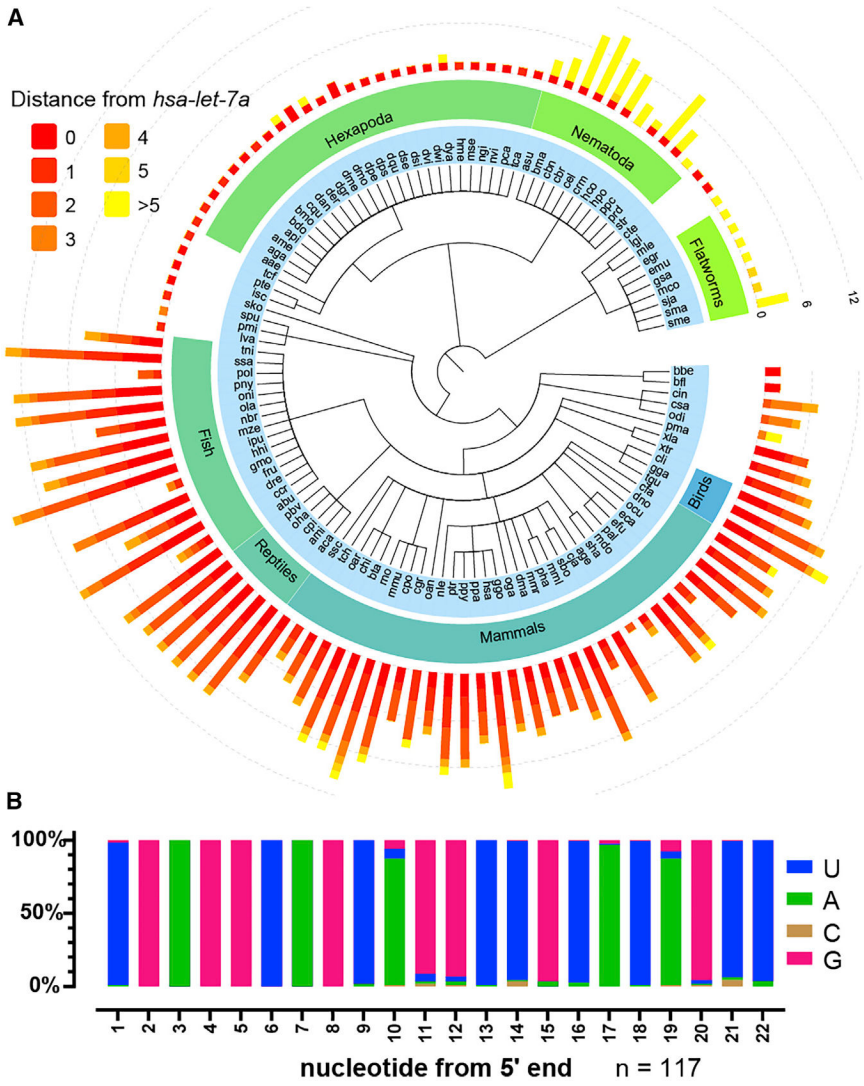

Figure 1. *let-7a* sequence is conserved across bilaterian species

(A) Summary of *let-7 family* miRNAs across bilaterian phylogeny. Bar length, number of *let-7 family* isoforms; bar color, sequence distance relative to *hsa-let-7a-5p*.

(B) Nucleotide frequency of the *let-7 family* isoforms most similar to *hsa-let-7a-5p* across bilaterians.

See also Figure S1.

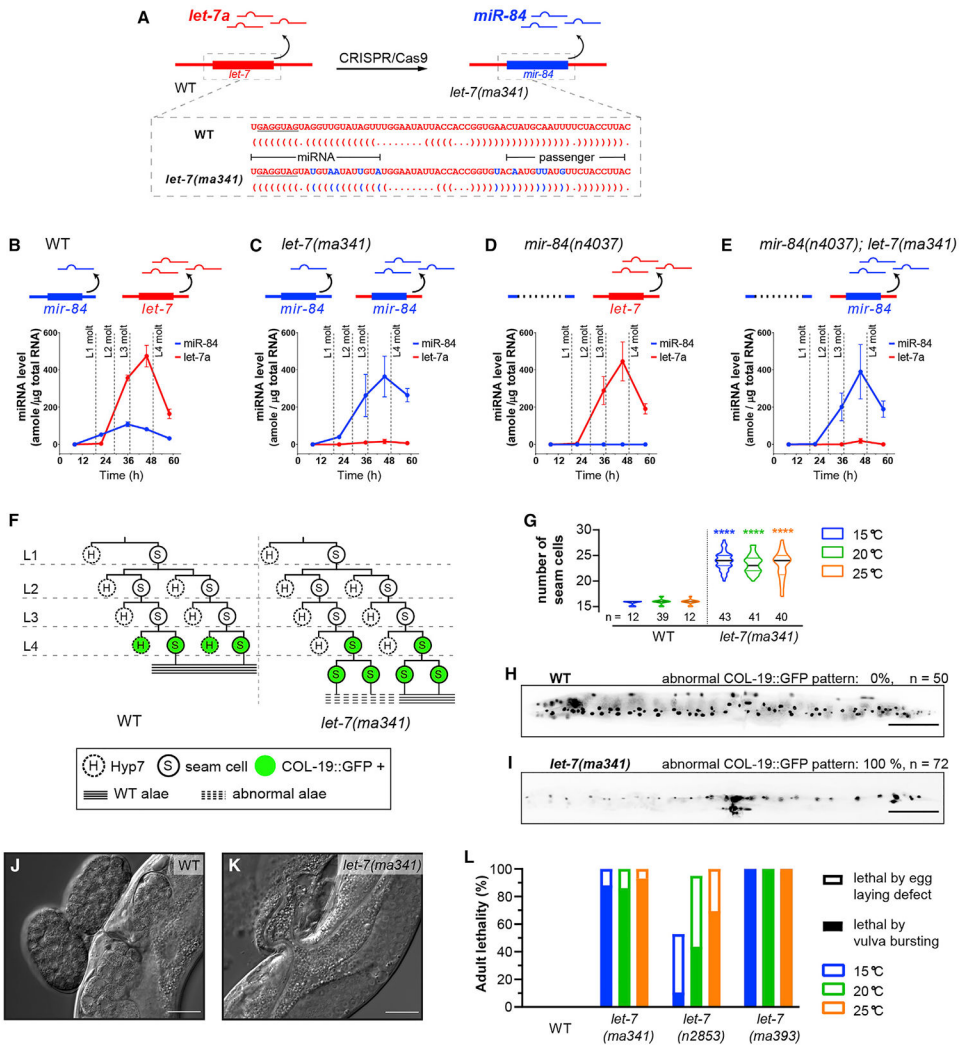

Figure 2. The 3′ non-seed sequence determines the functional specificity of *let-7a* among paralogs

(A) Strategy for generation of *let-7(ma341)* by CRISPR-Cas9-mediated swap of the *pre-let-7* sequence for the *pre-mir-84* sequence. Dot-bracket notations show the pre-miRNA structures predicted by RNAfold (Denman, 1993).

(B–E) Developmental profiles of *miR-84* and *let-7a* miRNAs by Fireplex assay. Expression is calibrated with synthetic *miR-84* and *let-7a* oligos. Time, hours after feeding starvation-arrested L1 larvae.

(F) Representative lineages and COL-19::GFP expression patterns of V1–V4 seam cells.

(G) Seam cell numbers of young adults. n, numbers of animals tested.

(H and I) Representative expression patterns of COL-19::GFP in adults. Scale bars, 100 µm.

(J and K) Differential interference contrast (DIC) images of the vulva region of adults. Scale bars, 25 µm.

(L) Adult lethality for wild type (WT), *let-7(ma341), let-7(n2853*, G5C), and *let-7(ma393, null)*. Lethal phenotypes are categorized as severe (via bursting of young adults through the vulva) or mild (via matricide of egg-laying-defective adults).

The data in (B)–(E) represent 3 biological replicas. Error bars indicate mean ± SD.

See also Figure S5. Details of the phenotypes are available in Table S1.

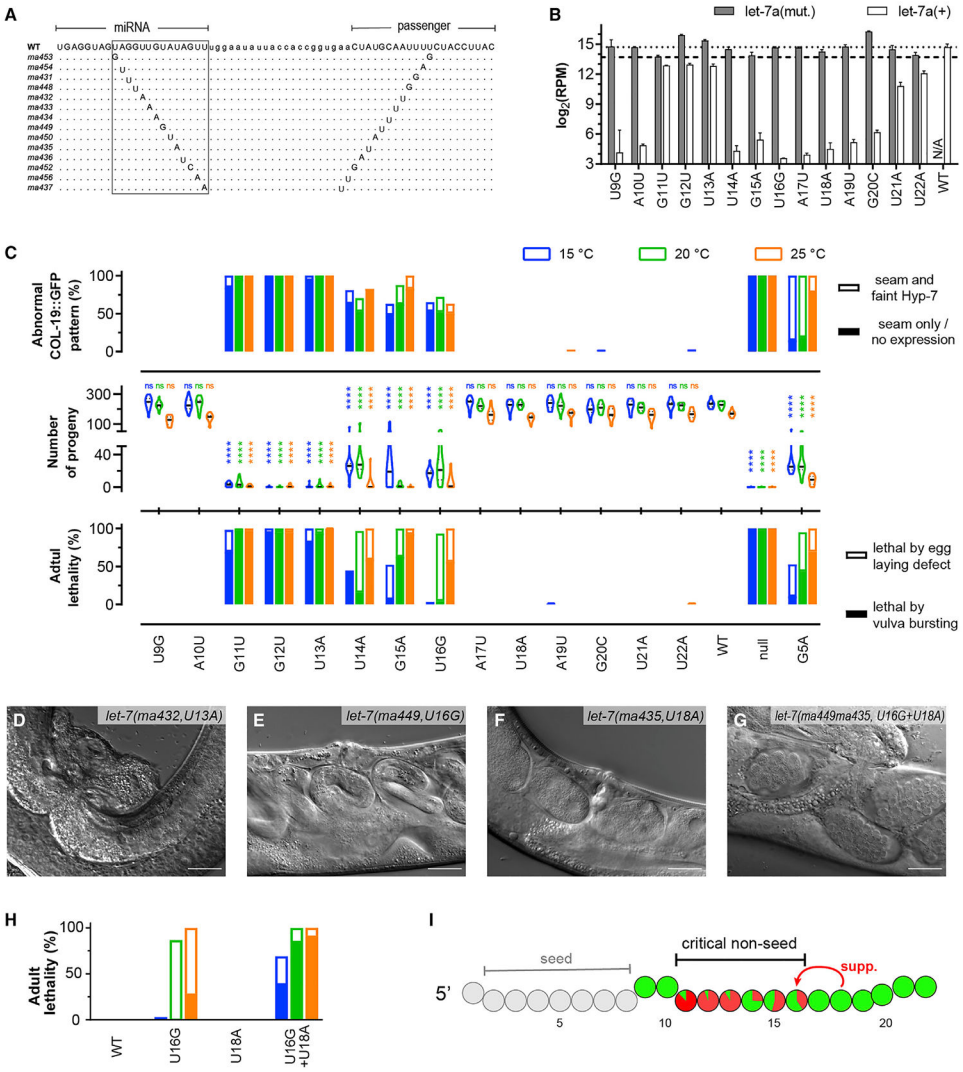

Figure 3. Contribution of single 3′ non-seed nucleotides to the *in vivo* function of *let-7a*

(A) Alignment of pre-miRNA sequences. Boxed 3′ non-seed regions.

(B) Small RNA sequencing reads from the L4 larvae that mapped to WT or mutant *let-7a* sequences for each single mutant. The reads mapping to WT *let-7a* for strains carrying mutations at g11–g13 include WT *let-7a* miRNA from balancer *umnIs25(mnDp1)*. The WT reads from U21A/U22A mutants likely reflect *let-7a(mutant)* miRNAs whose 3′ ends had been trimmed and subsequently uridylated *in vivo*, resulting in artificial *let-7a(+)* reads. Dashed lines, 100% (top) and 50% (bottom) of RPM of *let-7a(+)* in WT.

(C) Quantitation of *let-7a lf* phenotypes: percentage of animals with abnormal COL-19:GFP expression (top), numbers of progeny per animal (center), and percentage of adult lethality (bottom). Lethal phenotypes are categorized as in Figure 2L. Abnormal COL-19:GFP patterns are classified as no Hyp7 expression (severe) or faint Hyp7 expression (mild).

(D–G) DIC images of the vulva region in adults at 25°C. Scale bars, 25 μm.

(H) Functional synergy between g18 and the critical non-seed region based on vulva integrity defect. Labels are identical to (C) (bottom).

(I) Summary of the functional merits of *let-7a* 3′ non-seed nucleotides. Colored circle, 3′ non-seed nucleotide; red proportion, average adult lethality caused by vulva bursting at all temperatures.

Error bars indicate mean ± SD. See also Figures S2 and S3. Details of the phenotypes are available in Table S1.

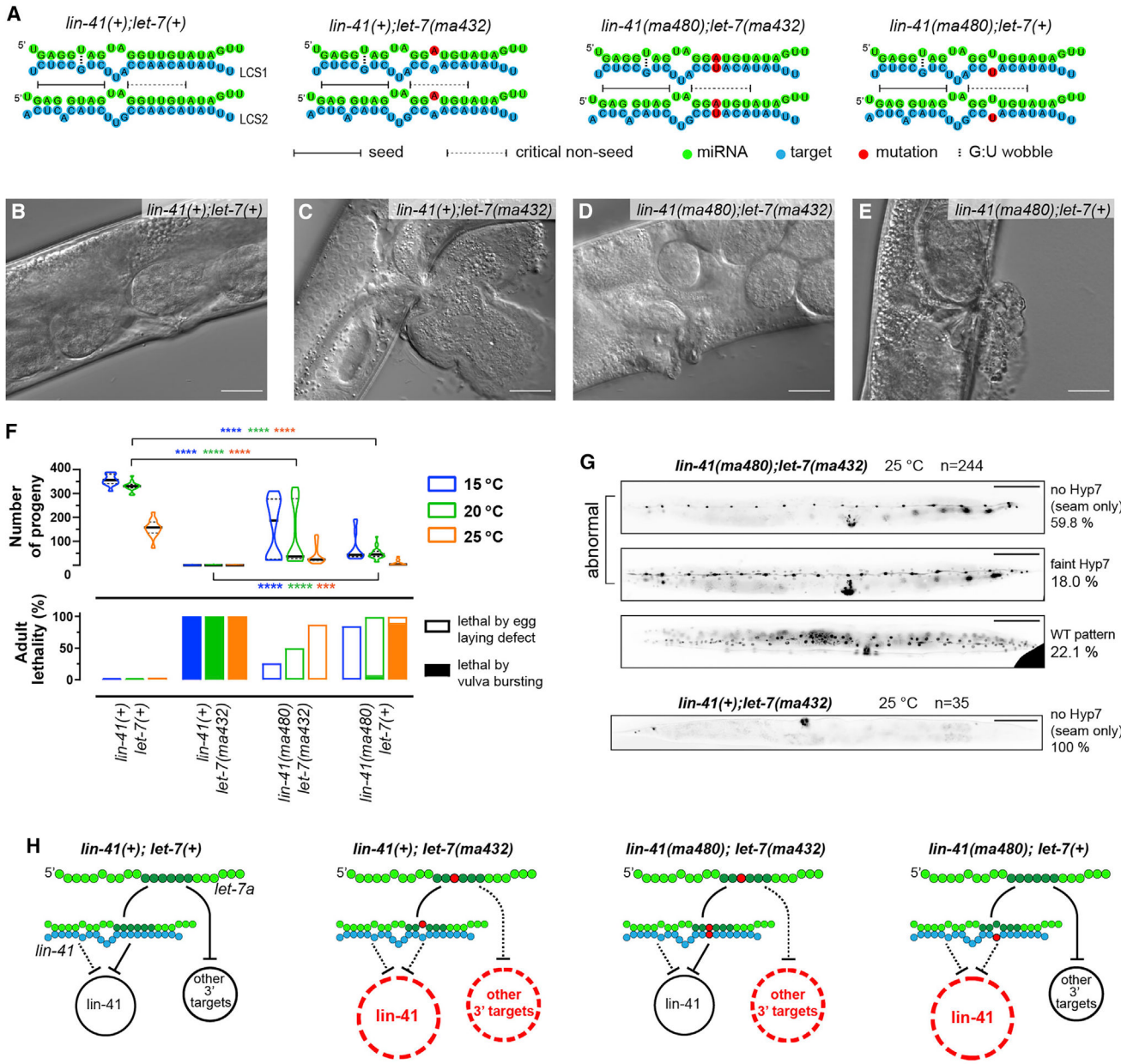

Figure 4. The *let-7a* critical non-seed nucleotides confer *in vivo* function by repressing *lin-41* and additional 3′ targets

(A) Pairing configurations between *let-7a* and *lin-41* LCS1/2.

(B–E) DIC images of adult vulva regions representative of the WT *lin-41(tn1541)* (B), *lin-41(tn1541);let-7(ma432)* (C), *lin-41(tn1541ma480);let-7(ma432)* (D) and *lin-41(tn1541ma480)* (E) at 25°C. Scale bars, 25 μm. All of the genotypes tested in this figure and in Figure 5 and Figure 7 include a GFP tag on LIN-41, denoted as *tn1541* (Spike et al., 2014).

(F) Vulva integrity defects reflected by adult lethality (bottom) and the number of progeny (top). Lethal phenotypes are categorized identically to Figure 2L.

(G) Representative COL-19::GFP pattern in young adults at 25°C. Scale bars, 100 μm.

(H) Models proposing that *lin-41* and additional 3′ targets are de-repressed in *let-7a* non-seed mutants.

See also Figure S4. Details of the phenotypes are available in Table S1.

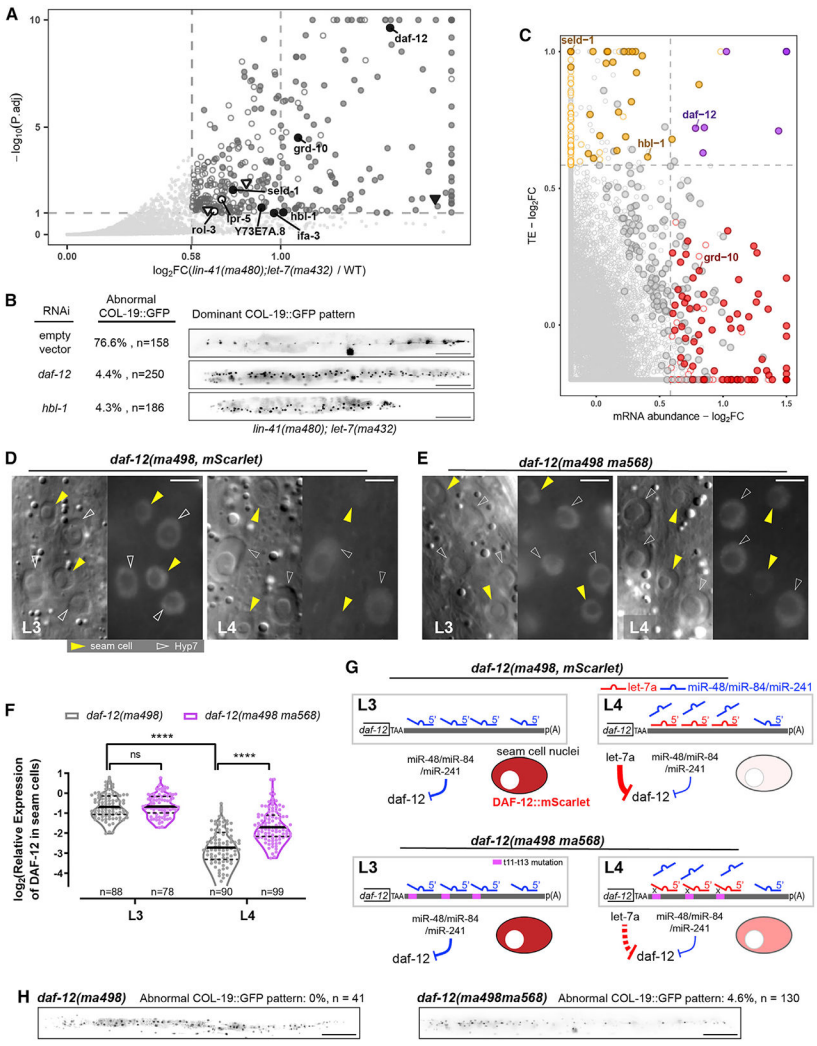

Figure 5. *let-7a* represses multiple targets, including *daf-12* and *hbl-1*, through 3′ non-seed pairing

(A) Differential expression analysis of translatomes of *lin-41(tn1541ma480);let-7(ma432)* and *lin-41(tn1541)*. Hollow points, developmentally dynamic genes for which the observed perturbation could be caused by asynchrony in staging between samples, independently of genotype; solid points, genes for which the observed perturbation is judged to likely reflect an effect of the *let-7a* mutation specifically (see STAR Methods; Table S3). Circular points with text labels, genes with predicted *let-7a* 3′ sites; triangle points, genes containing only *let-7a* seed-only sites.

(B) Retarded COL-19::GFP patterns characteristic of *lin-41(tn1541ma480);let-7(ma432)* young adults at 25°C under empty vector, *daf-12(RNAi)*, or *hbl-1(RNAi)*. Scale bars, 100 μm.

(C) Fold changes of mRNA abundance and translational efficiency (TE). Red points, genes with significantly increased mRNA abundance. Orange points, genes with significantly increased TE. Purple points, genes with both significantly increased TE and mRNA abundance. Circled points, genes with significantly increased RPFs in (A). Predicted *let-7a* 3′ targets are text labeled.

(D and E) DIC (left) and fluorescent (right) microscopy images showing expression of DAF-12::mSCARLET at L3/L4 stages at 25°C representative of *lin-41(tn1541);daf-12(ma498)* (D) and *lin-41(tn1541);daf-12(ma498ma568)* (E). Scale bars, 5 μm. All of the fluorescent images were generated with identical exposure and processing conditions.

(F) Quantification of relative fluorescent intensity of DAF-12::mSCARLET in seam cell nuclei relative to the adjacent Hyp7 nuclei. The numbers of seam cells quantified are shown under each violin plot. A total of 22 and 28 animals were scored for *daf-12(ma498)* at L3 and L4, respectively; 23 and 31 animals were scored for *daf-12(ma498ma568)* at L3 and L4, respectively.

(G) Models for *daf-12* repression at L3/L4. Purple region, trinucleotide mutations that disrupt duplexing with g11–g13 of *let-7a*.

(H) Representative expression patterns of COL-19:GFP in adult animals. Scale bars, 100 μm.

Data in (A) and (C) represent 3 biological replicas. See also Figures S6 and S7.

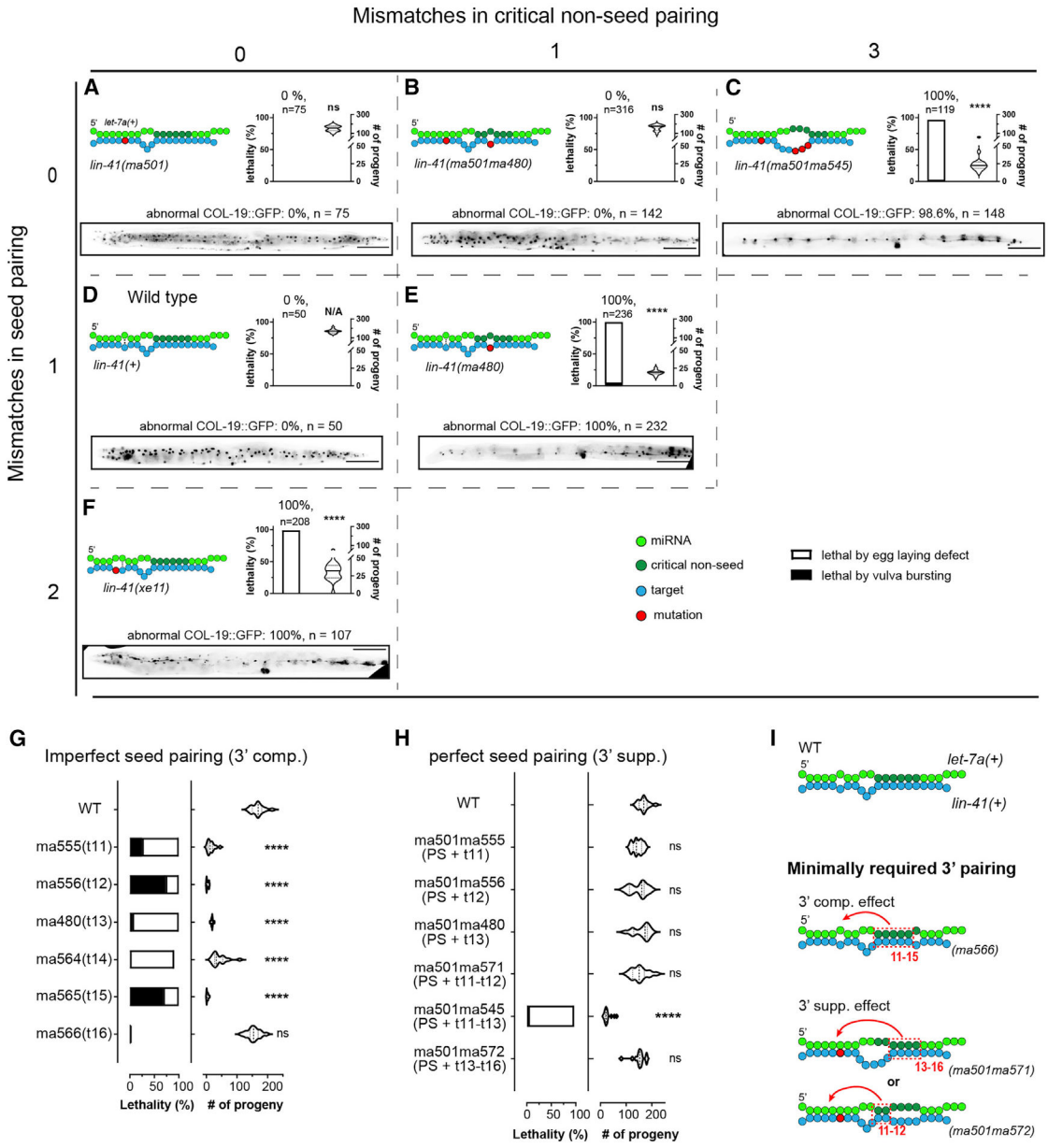

Figure 6. Critical 3′ non-seed pairing and seed pairing together contribute to *let-7a* target repression

(A–F) Pairing configurations of *let-7a* to the *lin-41* LCSs and associated phenotypes for *lin-41(ma501)* (A), *lin-41(ma501ma480)* (B), *lin-41(ma501ma545)* (C), *lin-41(+)* (D), *lin-41(ma480)* (E), and *lin-41(ex11)* (F), arranged in a matrix based on mismatches in seed (vertical axis) and critical non-seed region (horizontal axis). Each panel includes pairing pattern (top left), vulva defect (young adult lethality and number of progeny, top right), and heterochronic phenotype (bottom). Scale bars, 100 μm.

(G and H) Vulva integrity of *lin-41* LCSs mutants with 3′ pairing mismatches in the context of imperfect (G) and perfect seed pairing (H).

(I) Models depicting the minimal pairing requirement for 3′ compensatory and 3′ supplemental effects. Statistical significance indicates relative to WT. Phenotypes were

tested at 25°C. All of the *lin-41* alleles tested in this figure do not contain a fluorescent protein tag.

Details of the phenotypes available in Table S1.

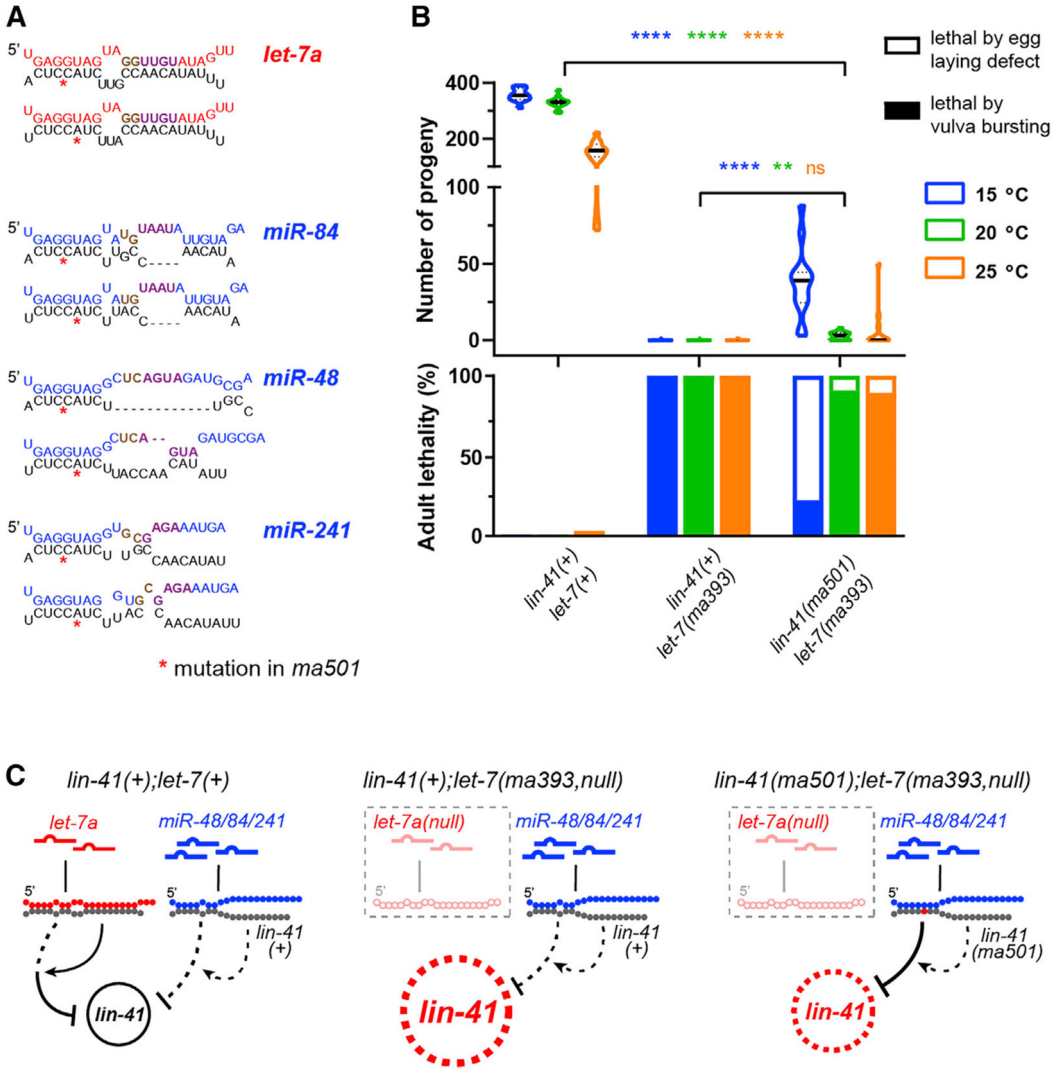

Figure 7. Perfect seed pairing alone is insufficient for *let-7a* family paralogs to confer full repression of *lin-41*

(A) Predicted seed-only pairing (RNAhybrid (Rehmsmeier et al., 2004) of *let-7a* and paralogs *miR-48/84/241* to LCS1 (top) and LCS2 (bottom) of *lin-41(ma501)*. Requirements for minimal supplemental pairing (t11–t12 pairing or t13–t16 pairing; Figure 6I) are indicated by brown or purple.

(B) Vulva integrity defects based on adult lethality (top) and number of progeny (bottom) in *lin-41(tn1541), lin-41(tn1541);let-7(ma393,null)* and *lin-41(tn1541ma501);let-7(ma393)*.

(C) Predicted targeting configurations.

Details of the phenotypes available in Table S1.

KEY RESOURCES TABLE

REAGENT or RESOURCE	SOURCE	IDENTIFIER
Bacterial and virus strains		
E.coli HB101	N/A	N/A
E.coli HT115 RNAi clones	Kamath et al., 2003	N/A
Chemicals, peptides, and recombinant proteins		
1X duplex buffer	IDT	Cat#11010301
QIAzol Lysis Reagent	Qiagen	Cat#79306
GlycoBlue	Invitrogen	Cat#AM9516
Protease Inhibitor Cocktail	Sigma-Aldrich	Cat#P2714
Turbo DNase	Invitrogen	Cat#AM2238
400 μm silica beads	OPS Diagnostic	Cat#PFAW-400-100-04
RNase I	Invitrogen	Cat#AM2294
SUPERase.In RNase Inhibitor	Invitrogen	Cat#AM2694
SYBR Gold Nucleic Acid Gel Stain	Invitrogen	Cat#S11494
T4 PNK	NEB	Cat#M0201S
RNase Inhibitor, Murine	NEB	Cat#M0314S
Thermostable RNase H	MCLAB	Cat#HTRH-100
Critical commercial cssays		
Q5 site-directed mutagenesis kit	NEB	Cat#E0552S
QIAseq miRNA Library kit	Qiagen	Cat#331505
QIAseq miRNA NGS 96 Index IL	Qiagen	Cat#331565
KAPA Library Quantification Kit	KAPA Biosystems	Cat#KK4824
RNA Clean & Concentrator-5 Kit	Zymo	Cat#R1015
NEBNext Multiplex Small RNA Library Prep Set	NEB	Cat#E7300
NEBNext Ultra II RNA Library Prep kit	NEB	Cat#E7775
NEBNext Multiplex oligo for Illumina	NEB	Cat#E7500 E7335 E7710 E7730
HiFiScript gDNA Removal cDNA Synthesis Kit	CWBIO	CW2020M
UltraSYBR Mixture (Low ROX)	CWBIO	CW2601L
Deposited data		
Raw and processed data of ribosome profiling	This paper	GEO: GSE171726
Raw and processed data of RNA-seq	This paper	GEO: GSE171733
Raw and processed data of small RNA seq	This paper	GEO: GSE171747
Code of target prediction algorithm	This paper	GitHub: https://github.com/IsanaVekslerLublinsky/Let7_Proj_code.git; Zenodo DOI: 6465945
C.elegans Reference Genome WBCel235	Ensemble/iGenome (Illumina)	https://support.illumina.com/sequencing/sequencing_software/igenome.html
miRBase release 22.1	miRBase	http://www.mirbase.org/ftp.shtml
Experimental models: Organisms/strains		
C.elegans: Strain N2	Caenorhabditis Genetics Center	WormBase Strain: N2

REAGENT or RESOURCE	SOURCE	IDENTIFIER
C.elegans: Strain VT1313 (*maIs105 V; mir-84(n4037) X*)	This paper	VT1313
C.elegans: Strain VT1367 (*maIs105 V*)	This paper	VT1367
C.elegans: Strain VT2692 (*maIs105 V; let-7(n2853) X*)	This paper	VT2692
C.elegans: Strain VT3439 (*maIs105 V; let-7(ma341) X*)	This paper	VT3439
C.elegans: Strain VT3455 (*wIs51 V*)	This paper	VT3455
C.elegans: Strain VT3460 (*wIs51 V; let-7a(ma341) X*)	This paper	VT3460
C.elegans: Strain VT3479 (*maIs105 V; let-7(ma341); mir-84(n4037) X*)	This paper	VT3479
C.elegans: Strain VT3585 *(lin-41(ma378) I; maIs105 V; let-7(ma341) X*)	This paper	VT3585
C.elegans: Strain VT3639 *(lin-41(ma378) I; maIs105 V)*	This paper	VT3639
C.elegans: Strain VT3645 *(mnDp1(umnIs25) (X;V),+/+, maIs105 V; let-7(ma393) X*)	Duan et al., 2020a; 2020b	VT3645
C.elegans: Strain VT3648 *(mnDp1(umnIs25) (X;V),+/+, maIs105 V; let-7(ma341) X)*	This paper	VT3648
C.elegans: Strain VT3729 *(mnDp1(umnIs25) (X;V),+/+, maIs105 V; let-7(ma432ma435) X)*	This paper	VT3729 ma432ma435 is also labeled as ma428
C.elegans: Strain VT3742 *(oxSi1091(Pmex-5::Cas-9(smu-2 introns) unc-119+) II; mnDp1(umnIs25) (X;V)/+ V; let-7(ma393) X)*	This paper	VT3742
C.elegans: Strain VT3793 *(mnDp1(umnIs25) (X;V),+/+,maIs105 V; let-7(ma431) X)*	This paper	VT3793
C.elegans: Strain VT3794 *(mnDp1(umnIs25) (X;V),+/+,maIs105 V; let-7(ma432) X)*	This paper	VT3794
C.elegans: Strain VT3795 *(mnDp1(umnIs25) (X;V),+/+,maIs105 V; let-7(ma433) X)*	This paper	VT3795
C.elegans: Strain VT3796 *(mnDp1(umnIs25) (X;V),+/+,maIs105 V; let-7(ma434) X)*	This paper	VT3796
C.elegans: Strain VT3797 *(maIs105 V; let-7(ma435) X)*	This paper	VT3797
C.elegans: Strain VT3798 *(maIs105 V; let-7(ma436) X)*	This paper	VT3798
C.elegans: Strain VT3799 *(maIs105 V; let-7(ma437) X)*	This paper	VT3799
C.elegans: Strain VT3825 *(mnDp1(umnIs25) (X;V),+/+,maIs105 V; let-7(ma448) X)*	This paper	VT3825
C.elegans: Strain VT3826 *(mnDp1(umnIs25) (X;V),+/+,maIs105 V; let-7(ma449) X)*	This paper	VT3826
C.elegans: Strain VT3827 *(maIs105 V; let-7(ma450) X)*	This paper	VT3827
C.elegans: Strain VT3828 *(maIs105 V; let-7(ma451) X)*	This paper	VT3828
C.elegans: Strain VT3829 *(maIs105 V; let-7(ma452) X)*	This paper	VT3829
C.elegans: Strain VT3835 *(maIs105 V; let-7(ma453) X)*	This paper	VT3835
C.elegans: Strain VT3836 *(maIs105 V; let-7(ma454) X)*	This paper	VT3836
C.elegans: Strain VT3843 *(maIs105 V; let-7(ma455) X)*	This paper	VT3843
C.elegans: Strain VT3844 *(maIs105 V; let-7(ma456) X)*	This paper	VT3844
C.elegans: Strain VT3867 *(lin-41(tn1541) I; oxSi1091 II; mnDp1(umnIs25) (X;V)/+ V; let-7(ma432) X)*	This paper	VT3867
C.elegans: Strain VT3868 *(lin-41(tn1541) I; mnDp1(umnIs25) (X;V)/+ V; let-7(ma432) X)*	This paper	VT3868
C.elegans: Strain VT3873 *(oxSi1091 II; mnDp1(umnIs25) (X;V)/+ V; let-7(ma432) X)*	This paper	VT3873
C.elegans: Strain VT3874 *(maIs105 V; let-7(ma476) X)*	This paper	VT3874
C.elegans: Strain VT3875 *(maIs105 V; let-7(ma477) X)*	This paper	VT3875
C.elegans: Strain VT3876 *(maIs105 V; let-7a(ma478) X)*	This paper	VT3876

REAGENT or RESOURCE	SOURCE	IDENTIFIER
C.elegans: Strain VT3877 *(mnDp1(umnIs25) (X;V),+/+, maIs105 V; let-7(ma449ma435) X)*	This paper	VT3877 ma449ma435 is also labeled as ma479
C.elegans: Strain VT3878 *(lin-41(tn1541ma480) I; let-7(ma432) X)*	This paper	VT3878
C.elegans: Strain VT3879 *(lin-41(tn1541ma480) I; maIs105 V; let-7(ma432) X)*	This paper	VT3879
C.elegans: Strain VT3945 *(lin-41(tn1541ma501) I; maIs105 V)*	This paper	VT3945
C.elegans: Strain VT3949 *(lin-41(tn1541ma480) I)*	This paper	VT3949
C.elegans: Strain VT3950 *(lin-41(tn1541ma480) I; maIs105 V)*	This paper	VT3950
C.elegans: Strain VT3954 *(lin-41(tn1541ma501) I; mnDp1(umnIs25) (X;V),+/+,maIs105 V; let-7(ma393) X)*	This paper	VT3954
C.elegans: Strain VT3959 *(lin-41(tn1541) I; mnDp1(umnIs25) (X;V),+/+,maIs105 V; let-7(ma393) X)*	This paper	VT3959
C.elegans: Strain VT3974 *(lin-41(ma501ma545) I; maIs105 V)*	This paper	VT3974 *ma501ma545* is also labeled as *ma511*
C.elegans: Strain VT3975 *(lin-41(xe11) I; maIs105 V)*	This paper	VT3975
C.elegans: Strain VT4009 *(lin-41(ma501ma572) I; maIs105 V)*	This paper	VT4009 ma501ma572 is also labeled as ma554
C.elegans: Strain VT4058 *(lin-41(ma501ma480) I; maIs105 V)*	This paper	VT4058 ma501ma480 is also labeled as ma504
C.elegans: Strain VT4060 *(lin-41(ma480) I; maIs105 V)*	This paper	VT4060
C.elegans: Strain VT4091 *(lin-41(ma501ma555) I; maIs105 V)*	This paper	VT4091 *ma501ma555* is also labeled as *ma552*
C.elegans: Strain VT4092 *(lin-41(ma501ma556) I; maIs105 V)*	This paper	VT4092 *ma501ma556* is also labeled as *ma553*
C.elegans: Strain VT4093 *(lin-41(ma501ma571) I; maIs105 V)*	This paper	VT4093 *ma501ma571* is also labeled as *ma554*
C.elegans: Strain VT4094 *(lin-41(ma555) I; maIs105 V)*	This paper	VT4094
C.elegans: Strain VT4095 *(lin-41(ma556) I; maIs105 V)*	This paper	VT4095
C.elegans: Strain VT4123 *(lin-41(ma564) I; maIs105 V)*	This paper	VT4123
C.elegans: Strain VT4124 *(lin-41(ma565) I; maIs105 V)*	This paper	VT4124
C.elegans: Strain VT4125 *(lin-41(ma566) I; maIs105V)*	This paper	VT4125
C.elegans: Strain VT4126 *(oxSi1091 II; maIs105 V; daf-12(ma498ma567) X)*	This paper	VT4126
C.elegans: Strain VT4128 *(lin-41(tn1541) I; maIs105 V; daf-12(ma498ma568) X)*	This paper	VT4128
C.elegans: Strain VT4129 *(lin-41(tn1541) I; maIs105 V; daf-12(ma498) X)*	This paper	VT4129
C.elegans: Strain DG3913 *(lin-41(tn1541) I)*	Caenorhabditis Genetics Center	WormBase: DG3913
Oligonucleotides		
see Table S6	N/A	N/A
Recombinant DNA		
Plasmid: pBlueScript SK(+) *let-7a(mir-84 swap)*	This paper	pBS-09
Plasmid: pCR2.1-TOPO *let-7a(U9G)*	This paper	pCR-32
Plasmid: pCR2.1-TOPO *let-7a(A10U)*	This paper	pCR-33
Plasmid: pCR2.1-TOPO *let-7a(G11U)*	This paper	pCR-12
Plasmid: pCR2.1-TOPO *let-7a(G12U)*	This paper	pCR-34
Plasmid: pCR2.1-TOPO *let-7a(U13A)*	This paper	pCR-25

REAGENT or RESOURCE	SOURCE	IDENTIFIER
Plasmid: pCR2.1-TOPO *let-7a(U14A)*	This paper	pCR-13
Plasmid: pCR2.1-TOPO *let-7a(G15A)*	This paper	pCR-14
Plasmid: pCR2.1-TOPO *let-7a(U16G)*	This paper	pCR-35
Plasmid: pCR2.1-TOPO *let-7a(A17U)*	This paper	pCR-36
Plasmid: pCR2.1-TOPO *let-7a(U18A)*	This paper	pCR-26
Plasmid: pCR2.1-TOPO *let-7a(A19U)*	This paper	pCR-15
Plasmid: pCR2.1-TOPO *let-7a(G20C)*	This paper	pCR-39
Plasmid: pCR2.1-TOPO *let-7a(U21A)*	This paper	pCR-40
Plasmid: pCR2.1-TOPO *let-7a(U22A)*	This paper	pCR-16
Plasmid: pCR2.1-TOPO *let-7a(U18C)*	This paper	pCR-37
Plasmid: pCR2.1-TOPO *let-7a(U18G)*	This paper	pCR-38
Plasmid: pCR2.1-TOPO *let-7a(U16G + U18A)*	This paper	pCR-41
Plasmid: pCR2.1-TOPO *let-7a(17–22)*	This paper	pCR-42
Plasmid: pCR2.1-TOPO *let-7a(A17U + U18A + A19U)*	This paper	pCR-43
Plasmid: pCR2.1-TOPO *let-7a(G20C + U21A + U22A)*	This paper	pCR-44
Plasmid: pCR2.1-TOPO *let-7(INPP4A, Jump Board, null)*	This paper	pCR-07
Software and algorithms		
let-7a target prediction algorithm	This paper	https://github.com/IsanaVekslerLublinsky/Let7_Proj_code.git Zenodo DOI: 6465945
ImageJ-FIJI	Schindelin et al., 2012	https://imagej.net/Fiji
Prism 8	GraphPad	https://www.graphpad.com/scientific-software/prism/
SnapGene Viewer	SnapGene	https://www.snapgene.com/snapgene-viewer/
Jalview2	Waterhouse et al., 2009	https://www.jalview.org/
Adobe Illustrator CS5	Adobe Inc.	https://www.adobe.com/products/illustrator.html
Cutadapt/1.9	Martin, 2011	https://cutadapt.readthedocs.io/en/stable/
Bowtie2/2.3.4.3	Langmead and Salzberg, 2012	http://bowtie-bio.sourceforge.net/bowtie2/index.shtml
STAR/2.7.6a	Dobin et al., 2013	https://github.com/alexdobin/STAR
featureCounts (Subread/1.6.2)	Liao et al., 2014	http://subread.sourceforge.net/
plastid/0.4.8	Dunn and Weissman, 2016	https://plastid.readthedocs.io/en/latest/index.html
DESeq2	Love et al., 2014	https://bioconductor.org/packages/release/bioc/html/DESeq2.html
RStudio(2019)	RStudio	https://rstudio.com/
ggplot2	Hadley, 2016	https://ggplot2.tidyverse.org/
Other		
SW 41 Ti swinging-bucket rotor	Beckman-Coulter	Cat#331362
Spin-X centrifuge tube filter	Millipore	Cat#CLS8160
Fisherbrand™ RNase-Free Disposable Pellet Pestles	Fisher Scientific	Cat#12-141-364